UiA University of Agder

Investigation of a PV System Using a Mathematical Model and Available Data

OLE-KRISTIAN MINDE NESE

SUPERVISOR
Anne Gerd Imenes

University of Agder, [2020]
Faculty of Engineering and Science
Department of Engineering Sciences

Master

Abstract

In this paper the investigation of a grid connected photovoltaic (PV) system equipped with module level DC-DC power optimizers is presented. The objective of this thesis is to investigate a PV system in a variety of mismatch conditions by creating a mathematical model with the ability to simulate it and to use this model to investigate the performance. The model will also in part be used to try and answer a research question, namely: Is it beneficial to equip a PV system with moduel level DC-DC power optimizers as opposed to a traditional string inverter with maximum power point tracking (MPPT).

A mathematical model was build based on an existing model and data regarding the PV system was collected from tigo.com were the power optimizers reports a value every minute.

The system was found to respond well to a number of mismatch conditions, mitigating them very successfully. However, in one instance the power optimizers were unable to allow the unaffected modules of a string to generate energy. Finally it was concluded that power optimizers have their benefit in a PV system, even without much mismatch.

For further investigation of the system several new experiments and economics calculations could be performed.

Preface

Background and motivation

I am a 26 year old male from Bergen, Norway. I have previously obtained a bachelors degree in Energy technology from the Western Norway University of Applied Sciences. My motivation for writing this dissertation is to investigate further a technology able to produce renewable energy from the sun, a technology that may become more and more important in the years to come.

The target group of this thesis is people with a desire to further understand a PV system and how a mathematical model of it can be constructed.

Acknowledgments

I would like to sincerely thank my supervisor Anne Gerd Imenes for providing me with necessary data to perform simulations, theoretical insight, enlightening discussions and meetings and for giving me constructive and helpful guidance. I would also like

to thank my parents for their continuous support regarding everything I do, and my sister for providing emotional relief during stressful situations in the form of making me laugh at things only you and I can comprehend. Finally, to all my friends who I can go climb, ski, and laugh with, thanks for reminding me that there exists a world beyond the confines of everyday life.

Decleration

1.	I/We hereby declare that my/our report is my/our own work and that I/We have not used any other sources or have received any other help than mentioned in the thesis.	☒
2.	I/we further declare that this thesis: - has not been used for another exam at another department/university/university college in Norway or abroad; - does not refer to the work of others without it being stated; - does not refer to own previous work without it being stated; - have all the references given in the literature list; - is not a copy, duplicate or copy of another's work or manuscript.	☒
3.	I/we am/are aware that violation of the above is regarded as cheating and may result in cancellation of exams and exclusion from universities and colleges in Norway, see Universitets- og høgskoleloven §§4-7 og 4-8 og Forskrift om eksamen §§ 31.	☒
4.	I/we am/are aware that all submitted theses may be checked for plagiarism.	☒
5.	I/we am/are aware that the University of Agder will deal with all cases where there is suspicion of cheating according to the university's guidelines for dealing with cases of cheating.	☒
6.	I/we have incorporated the rules and guidelines in the use of sources and references on the library's web pages.	☒

Figure 1: *Individual declaration*

Publishing Agreement

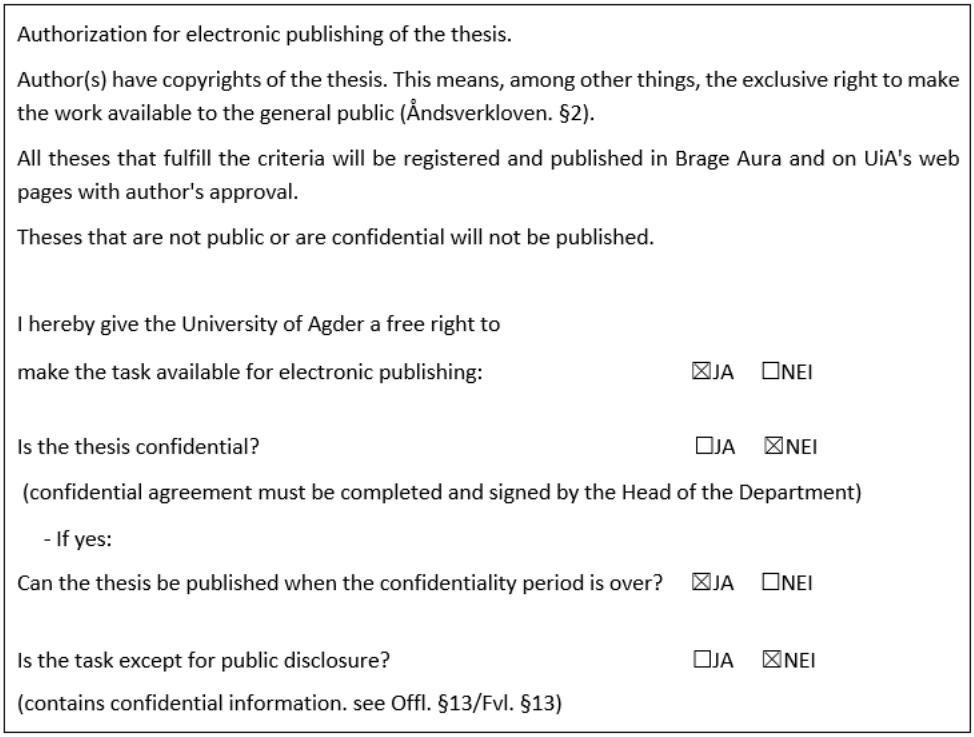

Authorization for electronic publishing of the thesis.

Author(s) have copyrights of the thesis. This means, among other things, the exclusive right to make the work available to the general public (Åndsverkloven. §2).

All theses that fulfill the criteria will be registered and published in Brage Aura and on UiA's web pages with author's approval.

Theses that are not public or are confidential will not be published.

I hereby give the University of Agder a free right to

make the task available for electronic publishing: ☒JA ☐NEI

Is the thesis confidential? ☐JA ☒NEI

(confidential agreement must be completed and signed by the Head of the Department)

- If yes:

Can the thesis be published when the confidentiality period is over? ☒JA ☐NEI

Is the task except for public disclosure? ☐JA ☒NEI

(contains confidential information. see Offl. §13/Fvl. §13)

Figure 2: *Publishing agreement*

Nomenclature

Abbreviations

AC	Alternating current
DC	Direct current
IV	Current-Voltage
MPP	Maximum Power Point
$MPPT$	Maximum Power Point Tracking

PIV	Predictive IV	
PV	Photovoltaic	
NOCT	Nominal Operating Cell Temperature	
STC	Standard Testing Conditions	

Constants

E_g	Band gap	1.12 eV
G_{noct}	Irradiance at nominal operating cell temperature	800 W/m^2
G_{stc}	Irradiance at STC	1000 W/m^2
k	Boltzmann Constant	$1.3805 \cdot 10^{-23} J/K$
q	Elemental Charge	$1.609 \cdot 10^{-19} C$
$T_{c,stc}$	Cell temperature at STC	25 C^o

Parameters

α	Temperature coefficient of current	$\%/K$
β	Temperature coefficient of voltage	V/K
η	Efficiency	
A	Ideality factor	
C_1	Coefficient	
C_2	Coefficient	
E	Energy	J
G	Irradiance	W/m^2
I	Current	A
I_n	Previous current value	A
I_p	Current of a solar module	A
I_s	Saturation current	A
I_t	Short circuit current based on irradiance alone	A
I_{mpp}	Current at maximum power point	A

I_{n+1}	Present current value	A
I_{pv}	Photocurrent	A
I_{sc}	Short circuit current	A
N_s	Number of cells	
P	Power	W
R_p	Parallel resistance	Ω
R_s	Series resistance	Ω
R_{PX}	Parallel resistance	Ω
R_{SX}	Series resistance	Ω
T_c	Cell temperature	C^o
T_{abs}	Absolute temperature	K
T_{air}	Air temperature	C^o
V	Voltage	V
V_p	Voltage of a solar module	V
V_t	Thermal voltage	V
V_{mpp}	Voltage at maximum power point	V
$V_{oc,m}$	Open circuit voltage for the considered irradiance	V
V_{oc}	Open circuit voltage	V
NOCT	Nominall operating cell temperature	C^o
SI	Shading Index	

Contents

1 Introduction

Renewable energy is in demand world wide and many technologies are rapidly growing, becoming more and more commercial. One such technology is based on the energy emitted from the sun and is known as solar cells. A variety of different technologies to convert solar energy to electric energy exists. The most commonly used technology is based on silicon, of which the most commonly type of cell is mono crystalline cells. They make up about 80 % of the market. There exists other technologies based on silicon such as poly crystalline cells [1].

Today, technology based on solar cells are becoming more and more commercial allowing individuals to install them on their own homes. The growth in the solar energy market is driven by the increase in environmental pollution affecting both the individual person and industries alike [2, 3].

The growing demand for solar energy gives rise to conditions unsuited for energy generation by the use of photovoltaics. Photovoltaic systems in urban environments are frequently exposed to shade, soiling and varying orientation that may gravely hinder the systems ability to produce power, especially when modules are connected together in strings and arrays. The solution is to introduce power electronic devices such as inverters and converters and utilizing distributed maximum power point tracking to mitigate electrical mismatch [4]. MMPT is an algorithm concerned with locating the maximum power point (MPP) of a system and a number of algorithms have been developed [5].

A mathematical model of such a system may be useful to study the characteristics of it. Several PV simulators and models have been proposed in recent years where the biggest development occurs for module level models that are either mathematical or circuital. Mathematical models are based on the physical equations of PV cells, while circuital models are implemented in specialized development software [6].

1.1 Research project

This thesis is a continuation of a research project from the fall of 2019 and dives further into the investigated system [7].

1.2 The various upcoming sections

In this report the basic theory concerning PV systems and the equations necesarry to build a mathematical model will be covered in Section 2. Furthermore, Section 3

is concerned with introducing the investigated PV system and the various explored scenarios. In addition, the methodology concerning the mathematical model for both a single model and a string is included. In Section 4 the results are presented and discussed, while in Section 5 a conclussion is drawn based on the results and research question. Finally, in Section 6 recommendations for further work is given.

1.3 Problem description

Module level DC-DC power optimizers are known to mitigate mismatch conditions. The energy saved by the power optimizers is known as reclaimed energy. Power optimizers from Tigo are supposedly able to do so quite successfully. How successfully they are able to reclaim energy and whether it is justifiable to employ them on every module rather than using a more traditional solution such as a inverter with string MPPT is the focus of this thesis.

2 Theory

2.1 Solar energy

The sun emits an enormous amount of energy in the form of radiation and can be considered a blackbody at $6000K$ [8, p. 5]. However, the radiation reaching the earth's surface is not consistent due to scattering and absorption of light in the atmosphere as well as the constant rotation. The constant rotation creates a varying path length through the atmosphere that varies with the time of day.

The radiation from the sun can be viewed as electromagnetic waves and it is the energy of these electromagnetic waves which solar panels exploits when producing electricity [8, p. 3].

2.2 Photovoltaic system

There exist a variety of different technologies to utilize the power produced by the sun. These are based on semiconductor materials of which silicon is the predominant and can be either monocrystalline, multicrystalline, polycrystalline, microcrystalline or amorphous. Monocrystalline silicon has an ordered structure and demonstrates predictable and uniform behaviour and is the ideal material to use when designing solar cells. The production of multi- and polycrystalline silicon is less expensive, but the expected power generation is lower than for monocrystalline silicon. Amorphous

silicon is cheaper to produce than multi- and polycrystalline silicon, but the use of it is mainly in non-critical outdoor applications or small consumer products [8, p 34-35].

The current produced by a solar cell is due to a photovoltaic effect caused in semiconductors when exposed to light. A semiconductor is a material that functions as an insulator when an insufficient amount of energy is present, but acts as a conductor when sufficient energy in the form of heat or light is present. The energy required to induce a photovoltaic effect is determined by the minimum energy necessary to transfer an electron from its covalent bond to its conduction band. This minimum energy is known as the *forbidden gap* [8, p. 31-33], or *energy band gap*.

The power generated in a solar cell is dependant on the induced current and voltage. Unfortunately, the two parameters are unable to operate at their individual maximum value at the same time. When the current operates at its maximum value the voltage value is zero, but if the voltage operates at its maximum value the current value is zero. The maximum current value occurs at short circuit conditions and is directly proportional to the amount of sunlight incident on the PV-array, while the maximum voltage value occurs at open circuit conditions and increases logarithmically with sunlight. The open-circuit voltage and the short-circuit current is also affected by the operating temperature of the solar cell. The operating temperature is influenced by the ambient air temperature, the characteristics of the module, the intensity of sunlight and wind. If the solar cell is subjected to a high operating temperature the short-circuit current will increase, while the open-circuit voltage will decrease. The decrease in open-circuit voltage is more significant than the increase in short-circuit current and a higher operating temperature will therefore lead to a decline in power generation [8, p 49-51].

The maximum power point of a solar cell is located somewhere in between the maximum values of the current and voltage. In Figure 3 [9] the relation between current and voltage in a solar cell also referred to as the IV characteristics is presented as well as the corresponding Power-Voltage curve [8, p 46].

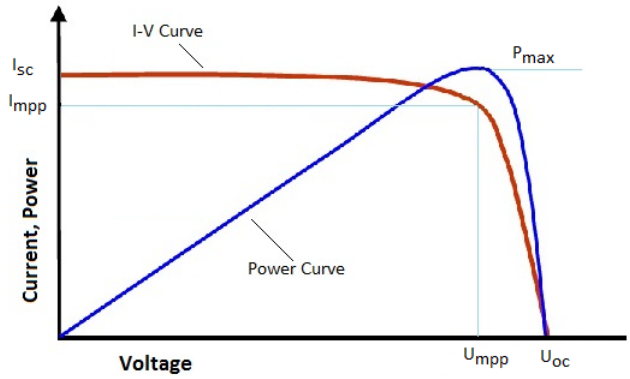

Figure 3: *IV and PV curve*

From Figure 3 it is possible to observe the previously discussed IV and Power-Voltage characteristics. When the current equals zero the voltage is at its maximum value and when the voltage is zero the current is at its maximum value. The maximum power point of both the current and voltage is presented in the figure. As can be seen, neither voltage nor current is operating at their individual maximum power point when the system is delivering maximum power. Any increase or decrease in either the voltage or currents maximum power point will result in a rapid decrease of produced power.

Such characteristics as presented in Figure 3 are often developed at standard testing condtitions (STC). At STC the irradiance is at 1000 W/m^2 and the cell temperature is given as 25 C^o [10]. Sadly, these conditions are hard to obtain outside a laboratory. In order to determine the two parameters either measurements or calculations can be used. Irradiance can be measured by the use of a Pyranometer [11], while the cell temperature can be measured at the back of the cells, or calculated at Nominal operating cell conditions (NOCT). NOCT are as presented in Tabel 1 [10].

Table 1: *Conditions defining the nominal operating cell temperature*

Conditions	**Value**
Irradiance	800 W/m^2
Air temperature	20 C^o
Wind speed	1 m/s
Mounting	Open back side

By using Equation 2.1 the actual cell temperature can be approximated.

$$T_c = T_{air} + \frac{NOCT - 20}{G_{NOCT}} G \tag{2.1}$$

Her T_c and T_{air} represents the cell and air temperature, NOCT represents the nominal operating cell temperature of the module provided in most PV datasheets, while G_{NOCT} and G is the irradiance at nominal operating conditions and the actual irradiance [10].

In order to significantly harvest power from the sun and provide better protection from environmental conditions a solar cell is connected to other solar cells in series and parallel to form a module. The series connected cells are connected as strings and behaves just as any other electrical circuit subjected to Kirchhof's law. This means that the current passing through each cell is equal hence the current produced by one cell will influence the other cells of the same string. It is common to have three strings or substrings per module which are connected in parallel and the total generated power is a result of the combined current and voltage formed by the arrays. Modules are similar to solar cells connected to other modules in strings and arrays and are also subjected to Kirchhof's law.

Due to the electric circuit behaviour of strings the behaviour of each solar cell can greatly affect the power production. If a cell produces a lower current than the other cells in the string it will force the other cells to perform at the same level. The difference in produced power can originate from shade, damaged cells, dust and so on. The difference between the maximum output and what actually is produced is called the mismatch loss. In order to minimize mismatch losses as much as possible identical cells are used to form the substrings of a module [8, p 75-77]. This can be attributed to modules as well so that identical modules are connected.

If a single cell in a string is subjected to poor operating conditions compared to the rest of the cells, hot spot heating can occur. This happens if the cells in the string approaches the short-circuit current of the afflicted cell. The unaffected cells continue to produce power that is then dissipated in the afflicted cell. This causes destructive effects such as cell or glass cracking and melting or degradation of the solar cell. In order to deal with this effect power electronics have to be implemented in the substrings of the module [12].

2.3 Power electronics

The destructive effect of hot spot heating may be avoided by the use of a power electronic device, namely a bypass diode. The bypass diode will allow current to "flow" through it instead of through the poor performing cell and so avoid hot spot heating. Ideally a bypass diode would be placed at each diode. However, due to the cost of bypass diodes they are usually placed on each string in a module. If a cell in a string is experiencing a significant decrease in produced power, the entire string will be "removed" from the module and cause a drop in the modules ability to generate energy. This will affect the other modules belonging to the same string, causing them to produce at a lower level as well [13].

To ensure that the maximum amount of energy is harvested from the sun a variety of power electronic devices can be included in a PV system. That is namely a DC-DC converter and/or inverter.

2.3.1 DC-DC converters

DC-DC converters are devices that convertes DC voltage and current to a different level. They are found in a variety of energy scenarios such as harnessing solar energy by the use of photovoltaics or increasing the efficiency of a compressor system. The DC-DC converters will influence a system by either increasing the voltage and so decrease the current or decrease the voltage and so increase the current. If the voltage is increased the converter boosts the voltage and such a converter is called a boost converter. On the other hand, if the voltage is decreased then a buck converter is applied. A converter with the ability to both increase and decrease the voltage is known as a buck/boost converter. The power can only flow in one direction through the various converters and they are therefore unidirectional [14, p 38].

2.3.2 Inverters

An inverter is a device that converts DC power to AC power. It does so by the use of power transistors and energy storing devices such as capacitors and inductors. The power transistor functions as a switch, turning the power on and off and along with the energy storing devices are able to create an alternating signal from a linear signal [15, 16].

The task of these power electronic devices is to ensure that the PV system produce at its maximum power point and applies a technique called maximum power point tracking.

2.4 Maximum Power Point Tracking

Maximum power point tracking is an integral part of a PV system and is usually performed by either an inverter, micro-inverter or a DC-DC converter. This is an electronic form of tracking that utilizes algorithms and control circuits to search for the maximum power point of the system [17]. The effect this have on the system depends on the amount of modules per power electronic device. If one such device is used to track the maximum power point of all the modules in a PV system a centralized MPPT is used and is typically performed by an inverter. This is the least expensive solution, but also results in the lowest performing module affecting the rest of system. A centralized MPPT solution should thus only be implemented in systems with a small degree of mismatch. If partial shading is present in the system it could lead to several modules experiencing different maximum power points. This leads to the need of several power optimizers to ensure that the different strings or modules can perform at their individual maximum power point. This is known as distributed MPPT [17].

The MPPT algorithm tracks either the produced voltage or current and depending on which parameter is tracked the MPP is located either when $\frac{dP}{dV} = 0$ or $\frac{dP}{dI} = 0$. The output of the algorithm provides a change in duty cycle of the inverter or converter, thus giving rise to a change in current and voltage values [18, 19].

Numerous MPPT methods have been developed where all rely on repeatedly changing either the voltage or current and observing the change in power [5]. The most common one is known as the Perturb and Observe method.

2.4.1 Perturb and Observe

The Perturb and Observe (PO) method is generally considered to be quite simple which is part of its attraction. It functions by continuously perturbing the reference value for either the current or voltage and then observing the change in power. This observed change is then used to inform the power electronic device performing the MPPT to shift the value of the tracked parameter towards the MPP.

In Figure 4 the flowchart of the Perturb and Observe method is displayed. Here $V(k)$, $I(k)$ and $P(k)$ describes the presently measured values where as $V(k-1)$, $I(k-1)$ and $P(k-1)$ describes the previously measured value [18].

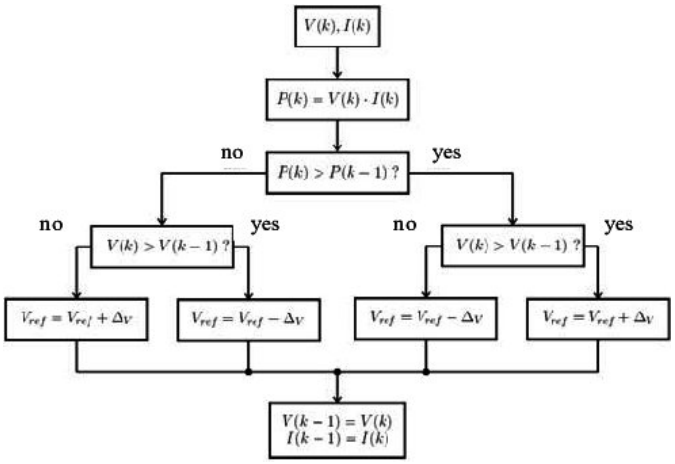

Figure 4: *Perturb and Observe flow chart*

From the figure it is possible to discern how the algorithm evaluates the different values by comparing the present value to the preceding one. Firstly, the present power value is compared to its previous value. No matter if the present power value is smaller or larger than the previous value, the voltage will be compared to its previous value. The outcome of this step results in a change in voltage. The change depends on relation between the present and preceding value.

There are a few drawbacks concerning this method the foremost being that it is unable to respond quickly to rapidly changing irradiance or temperature. In addition, the continued oscillation around the MPP due to the repeated change in voltage value causes power losses. Although small power losses are to be expected from an MPPT algorithm, these can prove large and significant even in steady-state condition with zero mismatch within the system [5].

2.5 Tigo

A company called Tigo which is a company creating optimizing solutions for PV systems have developed a technique to ensure the maximum energy harvest of a system. The technique is known as predictive IV and utilizes impedance matching and MPPT.

2.5.1 Predictive IV

Predictive IV (PIV) combines MPPT, impedance matching and historical module behaviour statistics. This is done to predict the optimum settings so that the system can generate the maximum amount of energy.

Due to advanced predictive capabilities the PIV parameters can be set locally, thus making it completely independent of any other module in the string as well as the inverter. This allows for very high speed monitoring and subsequently a high accuracy in real time response to variations in the perceived irradiation by the module.

PIV technology makes it possible to place optimizers on single modules in a string. This can reduce the number of optimizers necessary to produce at the MPP so that only modules afflicted by mismatch requires a power optimizer [20].

2.5.2 Impedance matching

Impedance matching is how the source and load impedances in an electric circuit are designed in order to transfer the desired power at the desired efficiency from the source to the load. If it is desirable to transfer the maximum amount of power the maximum power transfer theorem states that in direct current (DC) circuits the source resistance have to be equal to the load resistance, while the source impedance have to be equal to the complex conjugate of the load impedance in alternating current (AC) circuits. However, under these conditions a system would operate at an efficiency of 50%. It is not possible to maximize both efficiency and power transfer and a compromise will have to be made [21, 22].

The necessity of implementing impedance matching is to create a pathway around low performing modules to ensure to maximum performance. This process is visually represented in Figure 5 [23].

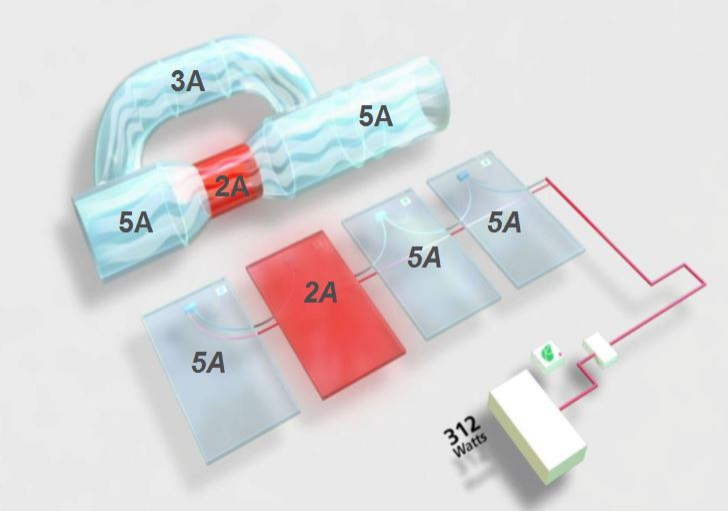

Figure 5: *How impedance matching is used to maintain the power production in*

As can be seen from the figure the high performing modules are able to perform at their maximum power point even though a low performing module is present in the string. The optimizing process is performed by a DC-DC optimizer and can be selectively distributed in the system where optimum results are seen at a per module level [24, 20].

2.6 Modelling of a PV system

There exists several different mathematical models in literature that describes the behaviour of a PV module. In the text below two different modelling methods will be investigated, namely the five parameter model and a simplified model.

2.6.1 The five parameter model

The five parameter model is able to provide a model of a photovoltaic system by using the parameters regarding the specific module provided by the manufacturer and general constants concerning the material used and physics. The methodology does in general involve either analytical, iterative or evolutionary methods. An iterative method is the method further investigated in this text and involves the Newton-Raphson function. This method is presented in several papers including in

[3], [25] and [6]. The method presented in [3] is the one further investigated in this report.

The five parameter model is also known as the single diode model and the equivalent electrical circuit is displayed in Figure 6 [3].

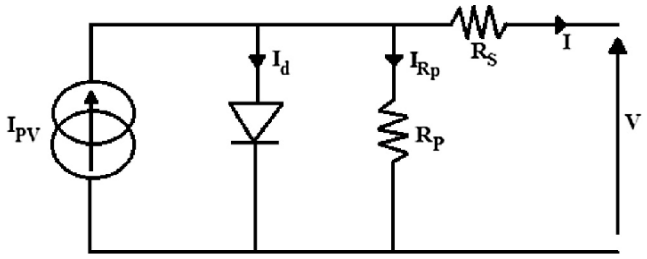

Figure 6: *Single diode model*

The five parameter model is so named because five separate parameters will have to be calculated. These are the photocurrent I_{pv}, saturation current I_s, ideality factor A, series resistance R_s and parallel resistance R_p. From Figure 6 it is possible to discern three of the unknown parameters. That is the photocurrent, series resistance and parallel resistance. The photocurrent, saturation current and parallel resistance can be calculated by the use of Equations 2.2, 2.3 and 2.4 [3].

$$I_{pv} = \frac{G}{G_{stc}}(I_{sc} + \alpha(T_c - T_{stc})) \tag{2.2}$$

$$I_s = \frac{I_{sc}}{exp(\frac{V_{oc}}{AN_sV_t}) - 1} \tag{2.3}$$

$$R_p = \frac{V_{mpp}(V_{mpp} + I_{mpp}R_s)}{I_{pv}V_{mpp} - V_{mpp}I_s exp(\frac{V_{mpp}+I_{mpp}R_s}{AN_sV_t}) + V_{mpp}I_s - P_{mpp}} \tag{2.4}$$

In Equation 2.2 G represents the actual irradiance, while G_{stc} represents the irradiance at STC in W/m^2. The I_{sc} term is the short circuit current and the α term is the current coefficient. Finally there are two temperature terms where the actual cell temperature T_c and the cell temperature at STC T_{stc} are compared.

The saturation current as described by Equation 2.3 is also dependant upon the short circuit current I_{sc}. In addition, it is dependant upon the open circuit current

V_{oc}, the ideality factor A, number of cells per module N_s and the thermal voltage V_t. The thermal voltage can be expressed as in Equation 2.5.

$$V_t = \frac{kT_c}{q} \tag{2.5}$$

Here k is the Boltzmann constant which have a value of $k = 1.3806 \cdot 10^{-}23\ J/K$, T_c is the cell temperature in Kelvin and q is the elementary charge constant $q = 1.609 \cdot 10^{-}19\ C$.

The series resistance is found through an iterative process which will be described later on. The ideality factor however, can be found by looking up values based on which PV technology is being used and can be found in Table 2 [26], or by the use of Equation 2.6 [3].

PV Technology	**A**
Si-mono	1.2
Si-poly	1.3
a-Si:H	1.8
a-Si:H Tadem	3.3
a-Si:H Triple	5
CdTe	1.5
CIS	1.5
GaAs	1.3

Table 2: *The ideality factor of various PV technologies*

$$A = \frac{\beta - \frac{V_{oc,stc}}{T_{stc}}}{N_s V_{t,stc}(\frac{\alpha}{I_{pv,stc}} - \frac{3}{T_{stc}} - \frac{e_g}{kT_{stc}^2})} \tag{2.6}$$

The only parameter in Equation 2.6 that has not previously been mentioned is the band gap e_g. The band gap and its properties have been described in Section 2.2.

These parameters are part of the characteristic equation concerning the single diode five parameter model as presented in Equation 2.7 [3].

$$I = I_{pv} - I_s[exp(\frac{V + R_s I}{A N_s V_t}) - 1] - \frac{V + R_s I}{R_p} \tag{2.7}$$

As can be seen from Equation 2.7 the current value is dependant upon itself, which is why an iterative method is required. If the Newton-Raphson method is considered, the expression to find the current is a combination of Equation 2.8 and 2.9

$$I_{n+1} = I_n - \frac{I_{pv} - I_n - I_s[exp(\frac{V+I_nR_s}{AN_sV_t}) - 1]}{-1 - \frac{I_nR_s}{AN_sV_t}[exp(\frac{V+I_nR_s}{AN_sV_t}) - 1]} \tag{2.8}$$

In Equation 2.8 the I_{n+1} term represents the new value, while the I_n term represents the previous value. I_n can be found throughout the use of Equation 2.9.

$$I_n = I_{pv} - I_s[exp(\frac{V + R_sI_{n+1}}{AN_sV_t}) - 1] - \frac{V + R_sI}{R_p} \tag{2.9}$$

In addition to the current and the five parameters previously mentioned, the number of cells per module N_s, voltage V and thermal voltage V_t is required to calculate the current through the module. N_s can be found in the module datasheet, the current is calculated through the entire voltage spectrum from $V = 0$ to V_{oc}.

To calculate the actual current and the two resistance terms some initial calculations of the photocurrent and the parallel resistance will have to be made. The initial calculations are based upon Equation 2.10 and 2.11 and is performed with STC values.

$$I_{pv,stc} = I_{sc,stc} \tag{2.10}$$

$$R_{p,min} = \frac{I_{mpp}}{I_{sc} - I_{mpp}} - \frac{V_{oc} - V_{mpp}}{V_{mpp}} \tag{2.11}$$

The initial series resistance will be considered to equal zero. That effectively makes the photocurrent the same as the short circuit current as in Equation 2.10. Equation 2.11 is not an exact value, but taken as an initial guess [3, 27] in order to initialize the iteration process.

These initial calculations along with assuming that R_s have an initial value of 0 is used to make the first iteration process possible. With these values the current is then calculated based on Equation 2.9 across the voltage spectrum of $0 - V_{oc}$. Then the power is calculated across the same voltage spectrum. When this computation is completed the difference between the given P_{mpp} and the calculated P_{mpp} is found.

This is called the error. If the error between the given and the calculated power value is less than 0.01 W, then the initial values of R_p and R_s is valid for further use. If that is not the case then a second set of calculations will have to be performed. In this case R_s is gradually shifted for each iteration and Equation 2.4 is used to locate R_p. In addition, the photocurrent is now calculated based on Equation 2.12 as opposed to 2.10.

$$I_{pv,stc} = I_{sc,stc}\frac{R_s + R_p}{R_p} \tag{2.12}$$

The current is still calculated by using Equation 2.8 and 2.9. Now the iteration process ends when the error term is less than 0.01. The two resistance terms R_s and R_p are then used in further calculations and at different irradiance and temperature levels. The authors in [3] states that the two resistances does change with irradiance and temperature, but in the majority of literature that is not accounted for and the values calculated at STC is used.

In order to make an effective model at any given irradiance and temperature some of the equations that where valid at STC conditions will have to be modified. The photocurrent, saturation current, short circuit current and open circuit voltage will now be expressed as in Equations 2.2, 2.13, 2.14 and 2.15 [3].

$$I_s = \frac{I_{sc,stc} + \alpha dT}{exp(\frac{V_{oc,stc}+\beta dT}{AN_sV_t})} + \frac{R_s(I_{sc,stc} + \alpha dT) - V_{oc,stc} - \beta dT}{R_p exp(\frac{V_{oc,stc}+\beta dT}{AN_sV_t})} \tag{2.13}$$

$$I_{sc} = I_{sc,stc} + \alpha(T_{stc} - T_c) \tag{2.14}$$

$$V_{oc} = \frac{AN_skT_c}{q} ln(\frac{I_{pv,stc}}{I_{s,stc}} + 1) \tag{2.15}$$

In addition, the saturation current at STC can now be calculated with Equation 2.16

$$I_{s,stc} = \frac{I_{sc,stc}(1 + \frac{R_s}{R_p})}{exp(\frac{V_{oc,stc}}{AN_sV_t}) - 1} \tag{2.16}$$

Finally the power produced can be found by multiplying the current I_{n+1} with the voltage as in Equation 2.17.

$$P = I_{n+1}V \tag{2.17}$$

2.6.2 Simplified model

A simplified mathematical model have been proposed in [28]. By using this method, the only parameters required are the ones provided by the manufacturer.

It locates the current I_P and voltage V_P of a solar module as in Equation 2.18 and 2.19.

$$I_P = I_{sc}[1 - C_1(e^{\frac{V_P}{C_2 V_{oc}}} - 1)] \tag{2.18}$$

$$V_P = V_{oc}C_2 ln[1 + \frac{1 - \frac{I_P}{I_{sc}}}{C_1}] \tag{2.19}$$

Since both of these equations depends on coefficients and values close to their maximum levels, these needs to be located. The short circuit current and the current at the MPP is proposed to be found by utilizing Equation 2.20 and 2.21.

$$I_{sc} = I_{sc,stc}\frac{G}{G_{stc}}[1 + \alpha(T - T_{stc})] \tag{2.20}$$

$$I_{mpp} = I_{mpp,stc}\frac{G}{G_{stc}}[1 + \alpha(T - T_{stc}] \tag{2.21}$$

The open circuit and the MPP voltage is found by utilizing Equation 2.22 and 2.23.

$$V_{oc} = V_{oc,stc} + \beta(T - T_{stc}) - \Delta V \tag{2.22}$$

$$V_{mpp} = V_{mpp,stc} + \beta(T - T_{stc}) - \Delta V \tag{2.23}$$

The ΔV part of the equation is included to find the difference in voltage due to irradiance and is found by comparing the open-circuit voltage at STC to the open-circuit voltage $V_{oc,m}$ for the considered irradiance as in Equation 2.24.

$$\Delta V = V_{oc,stc} - V_{oc,m} \tag{2.24}$$

The open-circuit voltage for the considered irradiance can be found by using Equation 2.25.

$$V_{oc,m} = C_2 V_{oc,stc} ln[1 + \frac{1 - \frac{I_t}{I_{sc,stc}}}{C_1}] \tag{2.25}$$

Here C_1 and C_2 are the same coefficients as in Equation 2.18 and 2.19. They can be located by applying Equation 2.26 and 2.27 as described in [28].

$$C_1 = (1 - \frac{I_{mpp}}{I_{sc}}) e^{\frac{-V_{mpp}}{C_2 V_{oc}}} \tag{2.26}$$

$$C_2 = \frac{\frac{V_{mpp}}{V_{oc}} - 1}{ln(1 - \frac{I_{mpp}}{I_{sc}})} \tag{2.27}$$

The two coefficients are dependent upon the actual short-circuit current, open-circuit voltage and the current and voltage corresponding to the maximum power point. I_t is the short-circuit current based on irradiance alone which can be found by utilizing Equation 2.28.

$$I_t = I_{sc} \frac{G}{G_{stc}} \tag{2.28}$$

Finally, the series resistance of the module can be included in the model by using Equation 2.29.

$$-R_s = (C_2 \frac{V_{oc}}{I_{sc}})(\frac{1}{1 + C_1}) \tag{2.29}$$

This is all well and good when considering a theoretical system, but in order to simulate an actual system two additional resistors are introduced. One which can be considered in parallel and one in series. The parallel resistance R_{PX} is determined by Equation 2.30.

$$R_{PX} = \frac{\Delta V_{sc}}{\Delta I_{sc}} \tag{2.30}$$

The ΔV_{sc} and ΔI_{sc} terms are in this instance located close to short circuit conditions. The series resistance R_{SX} is determined by Equation 2.31.

$$R_{SX} = \frac{\Delta V_{oc}}{\Delta I_{oc}} - R_s \tag{2.31}$$

When determining this resistance, the ΔV_{oc} and ΔI_{oc} are located close to open-circuit conditions. When these parameters are found, the actual current and voltage levels can be found by applying Equation 2.32 and 2.33.

$$I = I_P - \frac{V_P}{R_{PX}} \tag{2.32}$$

$$V = V_P - R_{SX} I_P \tag{2.33}$$

This model was created in order to enable the building of a mathematical system by only using the data provided by the manufacturer, without depending on parameters related to the PV technology.

2.7 Modelling strings

In order to model a string several modules will have to be connected together in series. Each module will have an individual input signal [6, 25] and can be modelled by using either one of the described mathematical models in the previous section. A bypass diode will have to be included in between each module.

In order to investigate the system when exposed to nonuniform operating conditions a shading index can be quite useful. A shading index can be created by comparing the energy produced by an actual system to a theoretical system with uniform operating conditions as shown in Equation 2.34 [29].

$$SI = 1 - \frac{E_{actual}}{E_{unshded}} \tag{2.34}$$

2.8 Literature review

The benefits of including power optimizers in PV-systems is well documented in [4, 30, 31, 29, 32, 33, 34]. The main gain from including power optimizers in PV-systems is to ensure the maximum energy yield through MPPT. This is particularly

useful when considering cases where mismatch is present in the system due to nonuniform operating conditions. In [4] [30] [31] [29] the effect of power optimizers under various operating conditions is explored. The common thread throughout these publications is that when there is close to zero mismatch within the system the power optimizers have no apparent effect, but as the mismatch increases so will the potential for reclaimed energy. There are different types of non-uniform operating conditions investigated in these publications of which partial shading, soiling, aging and orientation are the predominant factors. These affects a PV-system in various degrees and leads to a diverse amount of reclaimed energy. In [30] as much as 100% of the energy lost to mismatch from orientation within a string is found to be reclaimed by the use of power optimizers when the loss is between 1-20%. However, when the loss is due to partial shading the amount of reclaimed energy is reduced. When the partial shading is low the power optimizers are able to reclaim up to 70% of the loss, but as the energy loss increases the amount of reclaimed energy decreases and can be as low as 15%.

The amount of energy reclaimed by the power optimizers is also affected by how accurately the MPP is monitored in the system. In [31] three different MPPT scenarios are considered, namely centralized MMPT, distributed MMPT at module level and submodule MPPT. The different MPPT scenarios are simulted for two different mismatch conditions which are partial shading and ageing. It was found that for partial shading centralized MPPT did not have an apparent effect, while with distributed MPPT at module level resulted in an energy improvement of 2.17%-4.01%. With submodule MPPT the energy improvement was at 4.58% to 8.25%.

The addition of power optimizers in systems working in mismatched conditions has proven to be a beneficial inclusion. However, in [34] it is stated that in low mismatch systems the power optimizers can induce an overall negative effect due to power optimizers requiring power to function. According to [30] power optimizes are ineffective when considering a system of $100kW$ or more due to the high uniformity of such a system.

The power optimizing solution provided by Tigo as discussed in Section 2.5 has been tested in [29]. A system consisting of two modules were tested first by using a conventional method where both modules were connected to an inverter which performs MPPT and then by using Tigo module level dc-dc power optimizers. It was found that an annual increase in produced power of 5.8% was achieved when using Tigo's solution as opposed to the conventional method.

3 Method

3.1 System Information

The system investigated in this report is a grid connected PV system located on the roof of UIA campus Grimstad. The system consists of four different PV technologies where each technology is represented by 40 modules, resulting in a total of 160 modules, where the first modules were installed on 25.08.2018. The different PV technologies are grouped together to form strings and arrays, where only modules of the same technology are included. The modules are ordered in rows, where each module have a 10°tilt. However, each row is alternating in tilting 10°to the West and 10°to the East, giving the system an East-West orientation. This can be viewed in Figure 7.

Figure 7: *The PV system situated on the roof of UIA campus Grimstad*

Of the four different PV technologies, three are equipped with DC-DC power optimizers from Tigo. The three technologies are the IBC Solar poly-Si, IBC Solar mono-Si and the SunPower mono-Si. The technologies further investigated in this report are the two IBC Solar technologies. The reason being that they are most affected by shade, thus allowing for the investigation of the system when subjected to nonuniform operating conditions. The two IBC technologies are presented in Table 3 with their *STC* values as given in their respective manufacturer datasheet.

Table 3: *The values found in the manufacture datasheet of the two PV modules investigated*

Name	IBC Solar poly-Si	IBC Solar mono-Si
n_{cell}	60	60
NOCT	44 C^o	44 C^o
P_{mpp}	270 W	315 W
I_{sc}	9.08 A	10.02 A
V_{oc}	38.9 V	40.5 V
I_{mpp}	8.50 A	9.53 A
V_{mpp}	31.7 V	33.1 V
α	0.037 $\%/K$	0.06 $\%/K$
β	-0.13 V/K	-0.1134 V/K

As previously stated the individual modules are only connected to modules of the same technology in strings and arrays. In addition, the strings consists only of modules with the same orientation so as to prevent further mismatch. The number of modules in a string varies from technology to technology. The IBC Solar poly-Si modules have four strings with six modules and two strings equipped with eight modules, while the IBC Solar mono-si have eight similar strings containing five modules each. Both of the IBC technologies have modules with three substrings where each substring is protected by a diode. The string configurations can be viewed in Figure 8a and 8b where the modules with the same letter are in the same string.

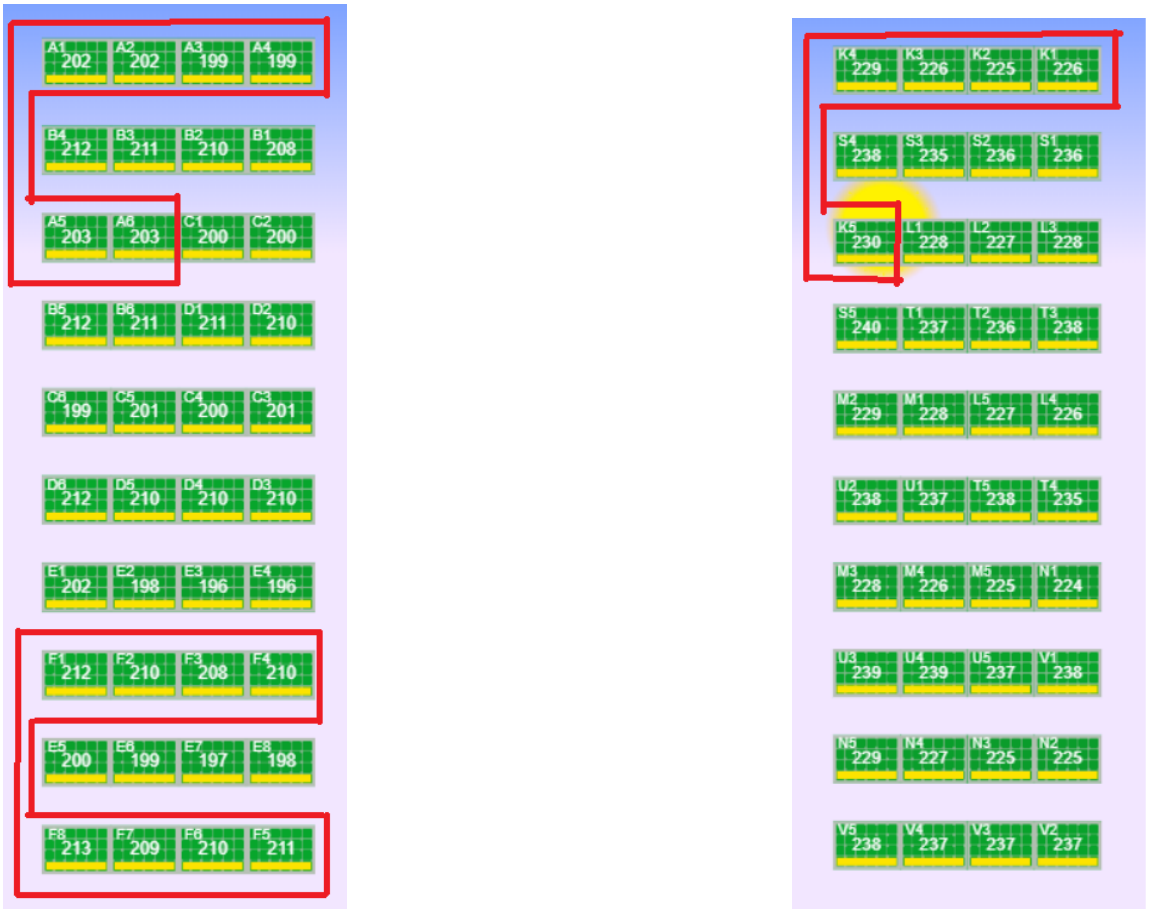

(a) *The string configurations of the poly-Si modules*

(b) *The string configuration of the mono-Si modules*

Figure 8: *Strings relating to the two IBC PV modules. The poly-Si modules have two different configurations, while the mono-Si modules have one string configuration.*

The outlined modules in Figure 8a and 8b are an example of how the various strings are configured.

The modules at the top row of Figure 8a and 8b are both tilted towards the East. The next row is then tilted towards the West. It alternates thus from top to bottom with the modules at the bottom facing West.

3.2 Data collection

3.2.1 Module data

Each module is equipped with a TS4 DC-DC power optimizer from Tigo, utilizing impedance matching and predictive IV as described in Section 2.4 in order to enable each module to operate at its individual maximum power point. In addition, the power optimizers are able to monitor the energy generation of the individual modules. The data reported by the optimizers are DC values, where the current, voltage and power is available for download on a per minute base. Furthermore, the total energy produced and reclaimed energy along with the current, voltage and power are available for observation at tigo.com.

The specifics of how the power optimizers perform the impedance matching and calculates reclaimed energy is patented by Tigo. The company is unwilling to share this information with the public, making it harder to predict the behaviour of the system.

Data concerning AC power as logged by the inverters is available from 30.01.2019, and reports value at every fifth minute. However, this data will not be used in this report.

3.2.2 Irradiance and temperature

Data concerning irradiance and temperature is gathered from on location measuring devices. The data used in this report concerns irradiance and ambient air temperature. These parameters are directly used in the mathematical model.

3.3 Mismatch

The potential mismatch factors that may affect the system can originate from a variety of sources. The origin of mismatch may arise from bird faeces, dust, shade from fence or solar tracker with solar irradiance instruments and damage to cells from rocks dropped by birds, manufacture faults, harsh handling or installation. Since the system still was still relatively young at the time this report was written, mismatch from aging was not likely to show any effect.

3.3.1 Dust and bird faeces

The accumulation of dust on modules could potentially lead to mismatch due to the module experiencing less irradiance than the modules it is in series with. In extreme

cases where entire strings are covered the produced power is significantly reduced, but there could potentially be no electrical mismatch within the system.

Bird faeces have been discovered on the modules which may also result in a reduced irradiance experienced by the influenced modules.

3.3.2 Shade from fence and solar tracker with solar irradiance instruments

The PV system on the rooftop of UIA campus Grimstad is for safety reasons surrounded by a fence as can be seen in Figure 7. The flip side of installing a fence is that it casts a shadow on the modules in its vicinity. The modules most affected by shade is displayed in Figure 9.

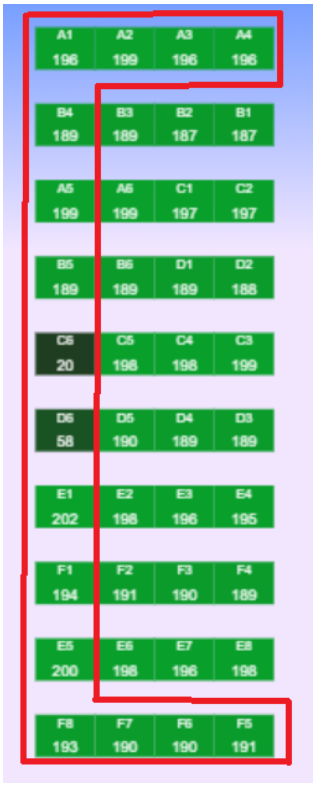

(a) *The modules affected by shade from the fence relating to the poly-Si technology*

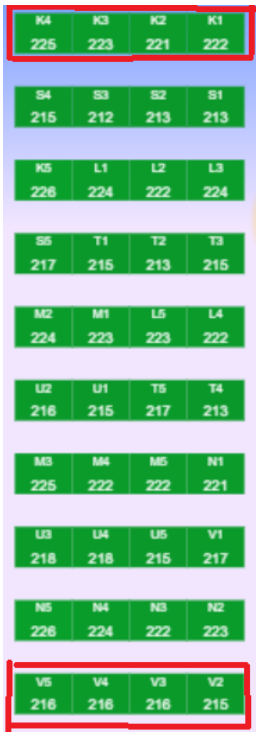

(b) *The modules affected by shade from the fence relating to the mono-Si technology*

Figure 9: *The various modules affected by shade from the surrounding fence*

The IBC Solar mono-Si modules are only affected by the shadow from the fence. The affected modules are shown in Figure 9b. As can be deducted, the modules affected by shade belongs to string K and V, leaving only one module in each string unaffected by shade. The poly-Si modules on the other hand is affected by both the fence as depicted in Figure 9a and by the solar tracker with solar irradiance instruments. There are in particular two modules that the solar tracker inflicts shade on. The two modules along with the string they belong to are depicted in Figure 10.

Figure 10: *The two modules mostly afflicted by shade from the pyranometer and the string they belong to*

In order to determine whether the DC-DC power optimizers are able to allow individual modules in a string to operate at its individual maximum power point, one of the strings affected by shade from the solar tracker with solar irradiance instruments was further investigated. This was string C, highlighted in red in Figure 10 and it was investigated on 11.03.2020 at 12:43 pm. The reason for investigating this day was that it shifted a lot between sunny and clouded sky, and it would therefore be interesting to see if the system would be able to cope with the changes in irradiance. The particular time of day investigated is due to the irradiance value being at its maximum. The power, voltage and current produced by each module is presented in Table 4

Table 4: *The power, voltage and current produced by each individual module in string C at 11.03.2020 12:43 pm, along with the irradiance and ambient temperature*

Module	Power	Voltage	Current	Irradiance	Temperature
C_1	145 W	32 V	4.53 A	535 W/m^2	8.8 C^o
C_2	146 W	32 V	4.56 A	535 W/m^2	8.8 C^o
C_3	146 W	32 V	4.56 A	535 W/m^2	8.8 C^o
C_4	146 W	32 V	4.56 A	535 W/m^2	8.8 C^o
C_5	145 W	31 V	4.68 A	535 W/m^2	8.8 C^o
C_6	59 W	36 V	1.64 A	535 W/m^2	8.8 C^o

The affected module is C_6 as can easily be deduced from Table 4. How this can be included in a mathematical model is described further below in Section 3.6.3.

The string will be modeled to fit three different scenarios. In one scenario it will not be affected by shade, while in the second scenario the string will be inflicted by shade, but being equipped with module level power optimizers. In the third and final scenario the string will be modeled as a traditional system with string inverter MPPT. This is done to visualize the difference between the two power electronic topologies and how much power is lost to shade.

3.3.3 Damaged cells

Birds have been observed to drop rocks onto the solar panels. Why they are doing so remains a mystery, but the possible damage they could inflict on the system can be quite extensive. As the system

3.4 Creating nonuniform operating conditions

An experiment was carried out by partially covering two modules and completely covering one module of the IBC Solar mono-Si technology. The covers were added to induce a shadow effect in order to observe how it would affect the power production of not only the covered module, but if the power optimizers would be able to maintain the energy production of the non-covered modules in the same string. The experiment was conducted from the 30. to the 31. of October. Several experiments were scheduled to be perfromed during the spring of 2020, but due to COVID-19 these experiments would not be allowed to be performed.

The different shading scenarios is presented in Figure 11, 12 and 13.

Figure 11: *The plastic covers a part of one substring on module M2*

Figure 12: *All three of module K5s substrings are covered*

Figure 13: *Module K4 is completely covered*

Figure 14: *The various modules the experiments were conducted on and the strings they belong to. The modules circled in yellow are the covered modules.*

The modules in Figure 12 and 13 are both connected to string K, while the module in Figure 11 is connected to string M. All of the covered modules are facing East, thus having the same orientation. Since the module in Figure 13 is completely covered by plastic it will adopt a behaviour where the module is shorted. The module in Figure 12 will adopt an equal behaviour since all three of its substrings are partially covered. However, only one of the substrings of module $M2$ is covered which should enable it to still generate energy.

3.5 Overall performance

The benefit of introducing power optimizers from Tigo to the system at module level is that they have the capability to mitigate mismatch present in the system.

This ability will allow the system to perform as well as possible. The energy saved or "reclaimed" is reported by the optimizers. In order to determine how much the power optimizers are able to reclaim the difference between the reported total energy and reported reclaim energy will be analysed.

The two IBC Solar mono-Si and poly-Si modules investigated will also be compared against each other by determining their specific power yield, where the energy generated throughout the year 2020 as of 07.06.2020 is compared against the power at STC. The energy produced in that space is presented in Table 5.

Table 5: *Energy produced by mono-Si and poly-Si modules from January 1. to June 7. 2020*

Name	Energy produced by an entire group	Energy produced by a single module
Poly-Si	4.47 MWh	119.32 kWh
Mono-Si	5.23 MWh	132.93 kWh

3.6 Modeling of a PV system

In order to compare the PV system to a hypothetical system without power optimizers, a mathematical model of the system would have to be created. The two mathematical methods discussed in Section 2.6 where both considered and a comparison between the two models would be necessary in order to determine which one to use. To do so they where both compared to the produced power from an actual module. The module in question was Module M1 and part of the M string previously discussed in Section 3.4. This particular module is made from mono-Si and facing east. In Table 6 the irradiance, ambient temperature, produced power, current and voltage by a mono-Si module at three different dates is presented.

Table 6: *The values of irradiance and temperature for the investigated days along with the actual power, current and voltage produced*

Time/date	**Irradiance**	**Temp.**	**Power**	**Current**	**Voltage**
11:08 30.10.19	259 W/m^2	4.74 C^o	88 W	2.56 A	34 V
12:43 11.03.20	535 W/m^2	8.8 C^o	165 W	5 A	33 V
11:57 19.05.20	839 W/m^2	13 C^o	249 W	8.03 A	31 V

The mathematical model chosen was the Five parameter model as previously described in Section 2.6.1, with the arguments for the selection of this method pre-

sented in Section 4.1.1. The equations and constants there described along with the values from the datasheets concerning the various PV technologies were written into $MATLAB$. The various constants used can be found in Table 7, while the values concerning the PV technologies is presented in Table 3 .

Table 7: *The various constants used when creating a mathematical model based on the five parameter model*

Constant	Name	Value
k	Boltzman's Constant	$1.3805 \cdot 10^{-23} J/K$
q	Elemental Charge	$1.609 \cdot 10^{-19} C$
e_g	Band gap for silicon	$1.12\ eV$
A_{mono}	Ideality factor for Si-mono	1.2
A_{poly}	Ideality factor for Si-poly	1.3
T_{stc}	Cell temperature at STC	$25\ C^o$
G_{stc}	Irradiance at STC	$1000\ W/m^2$

3.6.1 Modelling a single module

There were created two independent $MATLAB$ scripts per technology. The first script was created in order to determine the value of the parallel and series resistance as shown in Figure 6 at STC conditions, while the second script was constructed for the creating of IV and Power-Voltage curves from actual data and comparing it to the physical system. A common thread throughout the two scripts was that Equation 2.1 was used to calculate the operating temperature of the modules.

The first script was as just stated concerned with working out the value of R_s and R_p. This was achieved through a two step process. Initially, R_s was set to zero and Equation 2.11 was used to calculate an initial value of the parallel resistor R_p. Although finding the value of the two resistors was the main goal concerning this script, the three remaining parameters from the fiver parameter model would have to be calculated as well.

The three remaining parameters were the ideality factor A, photocurrent I_{pv} and the saturation current I_s. The value for the ideality factor was taken from Table 2 for the mono-Si modules, but calculated using Equation 2.6. The reason for this was that when simulated against actual data, this approach gave the most accurate values. I_{pv} and I_s was calculated by the use of Equation 2.2 and 2.3. In order to calculate the saturation current, the thermal voltage would have to calculated. This was done by the use of Equation 2.5.

In order to determine the current, an iteration process was utilized. This was the Newton-Raphson method. Equation 2.9 and 2.8 where the equations involved. The power was found by utilizing Equation 2.17.

The maximum calculated power would have to be compared to the given P_{mpp} for the specific PV technology. The calculated P_{mpp} was found using $MATLAB$s max function. If this comparison resulted in a difference between the given and calculated P_{mpp} exceeding the tolerance of 0.01, otherwise referred to as an error as described in Section 2.6.1, then a second set of calculations would have to be performed.

The second set of calculations are performed with a series resistance value which continuously change until the error becomes less than the tolerance value. Ideally, this would have been done with a loop function. However, due to the lack of access to a powerful computer given COVID-19 this would have to be shifted manually until a satisfactory result had been achieved. The parallel resistor will in this scenario be calculated by the use of Equation 2.4. The photocurrent is also calculated by the use of a different equation, namely Equation 2.12. Otherwise, the equations and process is similar to the process just described above. The simulation ends when R_s has obtained a value that yields an error value of less than the tolerance value. When this occurs, a second script will then be created with a new set of equations relating to the saturation current and other equations required to calculate it. In, addition the open circuit voltage V_{oc} for the given irradiance and temperature will be determined.

A second script was created in order to calculate values for actual operating conditions. The overall process to determine the current and power is quite similar to the process described for the first script. However, since this script was created to calculate values for actual operating conditions and not at STC, the equations used above would have to be modified to allow for not only changes in irradiance, but in temperature as well. This modification results in an increased amount of equations required to perform the calculations and relates to the photo- and saturation current. The equations now used to calculate these parameters are Equation 2.13 and 2.2. Equation 2.2 is only dependant upon values relating to the irradiance and the PV technology. The saturation current on the other hand, is in addition to being dependent upon temperature and material specific constants also reliant on the saturation current at STC conditions. However, the saturation current at STC is now determined by Equation 2.16. This is due to the predetermined resistance terms that will have to be included in order to present a realistic value of the saturation current. Furthermore, the open circuit voltage for the given irradiance and temperature was then determined by Equation 2.15. In addition, data regarding weather and irradi-

ance would be required in order to compare the mathematical model to the actual system.

In order to determine the accuracy of the mathematical model the maximum calculated power point was compared to the actual operational point of the PV modules.

The single module model will be used to investigate if a shaded module operates at the IV and power-voltage curve of unshaded modules. This is how the module level dc-dc power optimizers are supposed to function, allowing each module in a string to operate at its individual MPP and not in concert with each other.

The two *MATLAB* scripts are included in the Appendice B.

3.6.2 Creating strings

Since a mathematical model of a single module now has been implemented in *MATLAB*, the behaviour of a single module can be predicted/analyzed etc. However, since the PV system under investigation consists of strings, a model where the modules are series connected is of a paramount interest. The various modules connected together in strings in *Simulink* were build on the same principle as the single modules in *MATLAB*, namely the five parameter model. The model as constructed in *Simulink* and can be viewed in Figure 15 and 16.

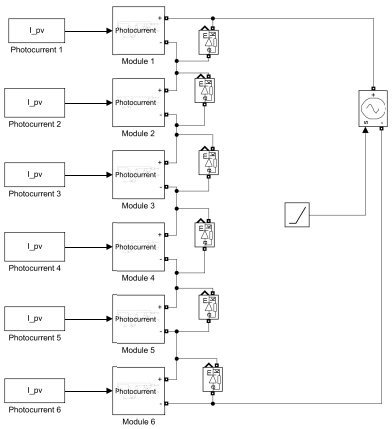

Figure 15: *Simulink model of a string relating to the poly-Si modules*

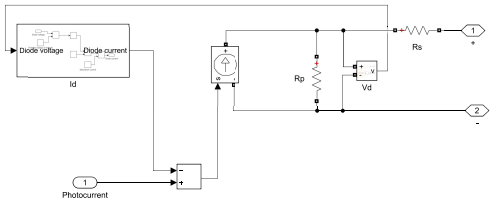

Figure 16: *The building blocks of a PV module in Simulink*

As can be viewed in Figure 15 each module has its own input signal. This input signal is drawn from the second $MATLAB$ scripts workspace and is the calculated photocurrent. The photocurrent then goes through the various components that are a part of the five parameter model, in other words; a diode and the series and parallel resistors. This is presented in Figure 16. Here the two resistors are easily implemented and recognized. However, the diode is simulated by the use of the second term from Equation 2.7 which relates to the current through the diode and not a simulink model of a diode. This is due to diodes in the simscape environment only providing linear diodes. This does not fit well when simulating PV modules as they have an exponential behaviour, and this was then simulated by a diode since they have a similar exponential behaviour. The diode current is dependant on voltage. This voltage is the same as the voltage over the parallel resistor and is because the two components are parallel connected. That voltage across the parallel resistor is therefore used to calculate the diode current.

The various components included in determining the diode current in Figure 16 is included in Appendice A.1.

3.6.3 Modelling mismatch

Since mismatch conditions occur in the system, mismatch also have to be included in the the model as it is vital for determining how strings actually operate. In the system investigated in this report, the majority of mismatch originates from shade

inflicted on the system by the surrounding fence. The shade was included in the mathematical model by creating a shading index. Since the system was investigated at specific times the shading index would be calculated at the desired time of day by comparing the power produced by a shaded module to an unshaded module. This approach differs from the one described in Section 2.7 in that it does not account for the difference of produced energy over a certain period of time, but looks at the power produced at a specific time. Thus, the equation becomes as in Equation 3.1.

$$SI = \frac{P_{shade}}{P_{unshade}} \tag{3.1}$$

This value is then further used when determining the power produced by shaded modules in the mathematical model by adding the shading index to the calculated photocurrent. This was done to visualize how much energy could potentially be lost if the system was not equipped with module level power optimizers. A demonstration of how the Simulink model performs when subjected to mismatch conditions is displayed in Figure 17, with an visual representation in 18 of how this could be implemented.

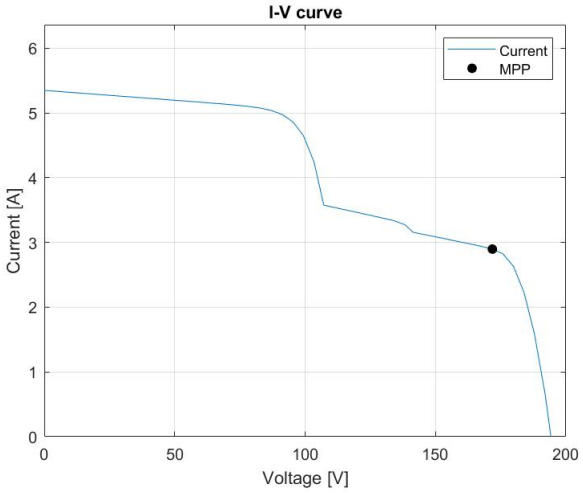

Figure 17: *How the current behaves when a string without module level power optimizers is subjected to mismatch*

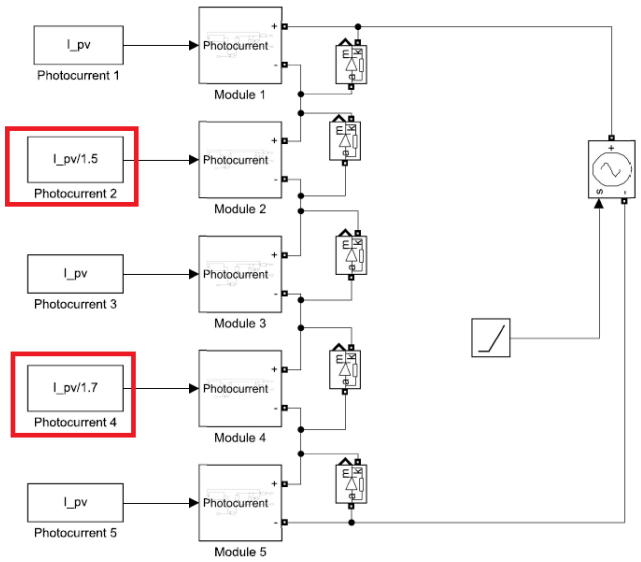

Figure 18: *An example of how shading conditions was implemented in the Simulink model.*

Since modules equipped with module level power optimizers from Tigo should in theory be able to mitigate mismatch this would have to be included. In the mathematical model this was done by adding the calculated currents, both shaded and unshaded and then diving by the number of modules in the string.

An IV curve will be constructed for an unshaded module using available data regarding irradiance and module temperature. A calculated maximum power point will be calculated for the IV curve and compared to the actual operating point of the unshaded modules. The shaded module will also be compared to the IV curve to see whether it falls on it, or operates with an independent IV curve.

4 Results

4.1 Mathematical model

4.1.1 Single diode model vs Simplified model

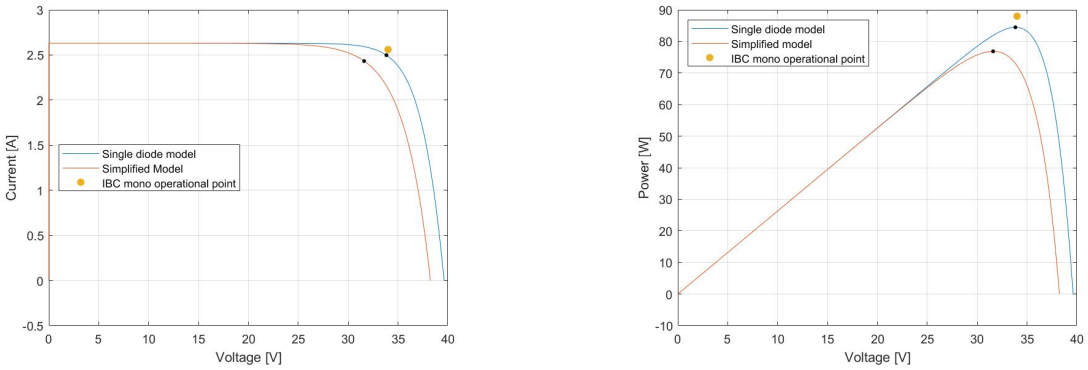

(a) (b)

Figure 19: *IV and Power-Voltage curves created to determine the accuracy of the Single diode and Simplified model on 30.10.2019*

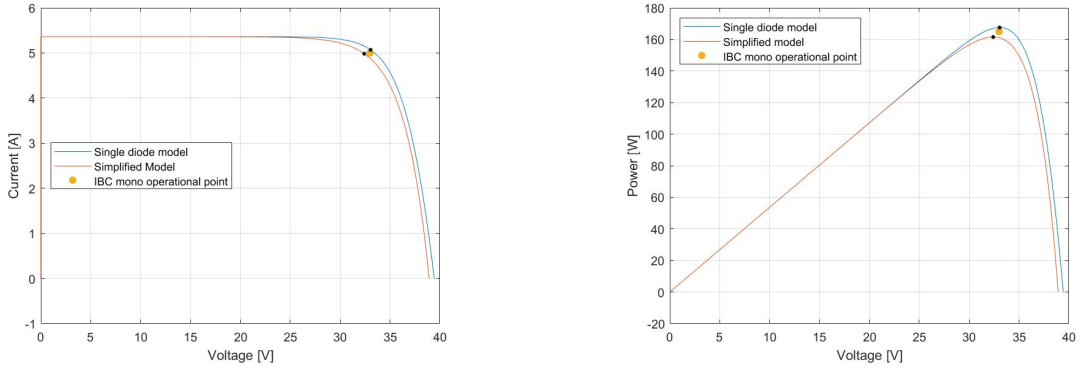

(a) (b)

Figure 20: *IV and Power-Voltage curves created to determine the accuracy of the Single diode and Simplified mode on 11.03.2020*

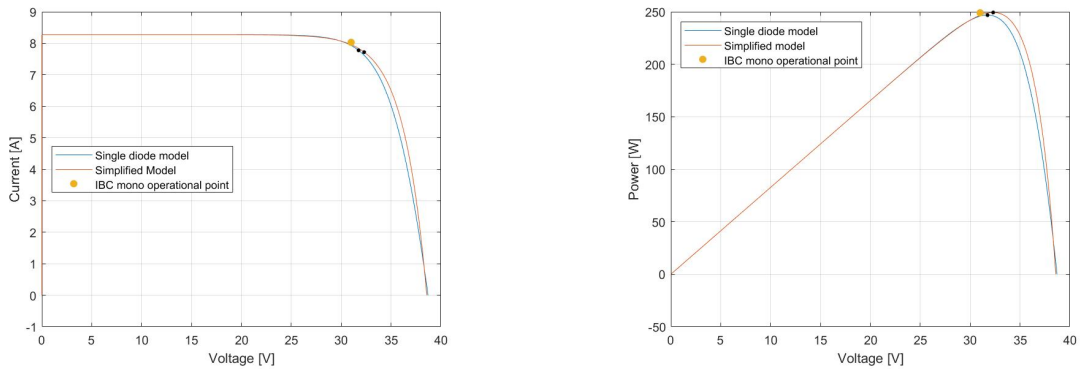

(a) (b)

Figure 21: *IV and Power-Voltage curves created to determine the accuracy of the Single diode and Simplified model on 19.05.2020*

As previously mentioned in Section 3.6 the single diode model was chosen as the preferred mathematical model. In Figure 19, 20 and 21 the IV and Power-Voltage curves for the three different dates and times presented in Table 6 are displayed.

In Figure 19 neither of the two models are able to accurately determine the operating point of the actual module. However, the single diode model is the most accurate of the two. When inspecting the Figure 20 and 21, the behaviour of the different models adopts a more similar behaviour and estimates a MPP in closer proximity to each other and the actual operating point. The common thread throughout these figures is that the single diode model displays a MPP more in tune with the actual data. Nevertheless, it is worth noticing that the Simplified model becomes more accurate with increasing irradiance and from Figure 21b it is possible to discern that it is able to quite accurately predict the produced power. However, when studying Figure 21a one can observe that it predicts the voltage and current values quite different from the ones reported by Tigo.

A benefit of using the five parameter model is that it enables an investigation of several attributes of the material used, such as the ideality factor, parallel resistor and series resistor. This allows for a closer study of how various components may affect the power produced in a PV system. This would not be possible in the Simplified model, where the only parameters that can be changed manually are the irradiance and the operating temperature.

4.1.2 Calculated parameters

In Table 8 the estimated fixed parameters necessary to perform the Single diode model is presented.

Table 8: *Estimated fixed parameters for the IBC Solar mono-Si and poly-Si modules*

Name	Mono-Si	Poly-Si
R_s	0.1976 Ω	0.2331 Ω
R_p	109.2119Ω	76.602 Ω
A	1.1059	1.0836

There is a small difference between the calculated ideality factors. This implies that the poly-Si modules are able to operate in closer harmony with the ideal IV curve. As mentioned in Section 3.6 the ideality factor for the poly-Si modules was based on the calculated value, while for the mono-Si modules the value provided in Table 2 was used. This was due to the mono-Si modules operating more in concert with the actual data when using the given value as opposed to the calculated value. The implications are that the mono-Si modules are unable to operate as closely to their ideal IV curve as the poly-Si modules, and also less then their own potential based on the calculated value of the ideality factor.

4.2 Shade from solar tracker with solar irradiance instruments

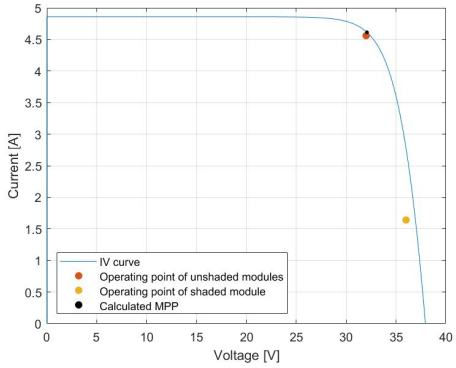

(a) *IV curve of the poly-Si module along with the operating point of both a shaded and unshaded module*

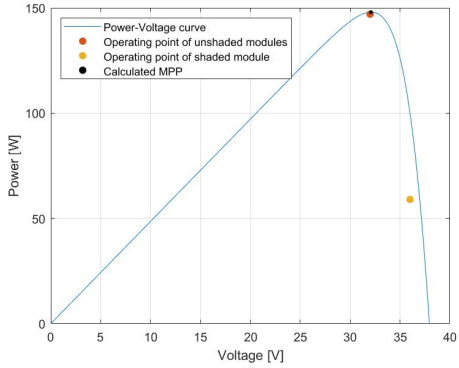

(b) *Power-Voltage curve of the poly-Si module along with the operating point of both a shaded and unshaded module*

Figure 22: *IV and Power-Voltage curves on the 11.03.2020*

By examining Figure 22a and 22b the calculated IV and Power-Voltage curve for a single unshaded module of string C given the conditions set in Section 3.3.2 is presented along with the operating point of unshaded and shaded modules. As can be seen, the calculated MPP is quite similar to the actual operating point of the unshaded modules. It is possible to detect that the shaded module operates outside the estimated curves of the unshaded modules, even though the investigated modules are connected to the same string. This is in agreement with how the power optimizers are supposed to operate, allowing each module to operate at its individual MPP.

The shaded module operates with a higher voltage than the unshaded module. This could be due to it being exposed to a lower degree of irradiance, thus causing a lower operating temperature which allows for a higher operating voltage. Given that the module operates with a high voltage, it is logical to assume that the shade inflicting the module is not sever enough to enable hot spot heating to occur, forcing a bypass diode or fuse to disengage a substring, making the substring unable to contribute power. It is collaborated by the fact that the current is operating at a low value, as the current is more dependent upon irradiance than the voltage is. This operating point is caused by the MPPT algorithm. It is possible that it is able to recognise that a higher operating voltage for the given circumstances is prefered.

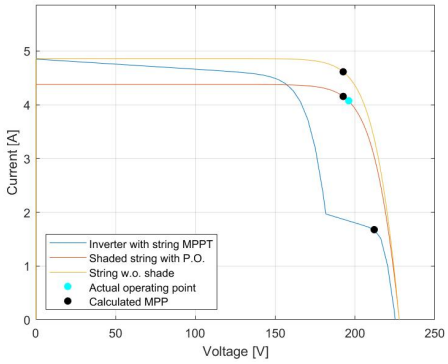

(a) *Iv curves concerning the various behaviour for the investigated string*

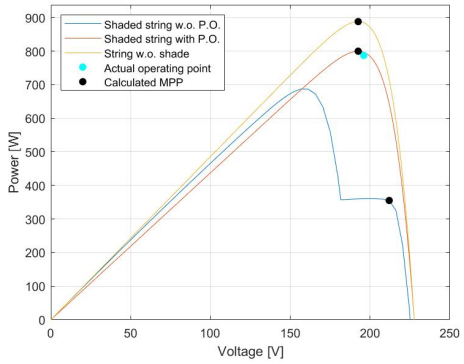

(b) *Power-Voltage curves concerning the various behaviour for the investigated string*

Figure 23: *Shows how a string reacts for different scenarios. Namely, when not shaded, when exposed to shade but equipped with module level power optimizers and when unequipped.*

In Figure 23a and 23b the simulation of a PV string for the different scenarios previously mentioned in Section 3.3.2 is displayed. The curve representing the actual string, with shade and module level DC-DC power optimizers have a calculated MPP similar to the actual operating point, just as in Figure 22a and 22b.

The shaded string with power optimizers is supposed to mimic the behaviour of the actual system. However, it is possible to see from both figures that there exist a difference between the calculated MPP and the actual operating point. This can be due to temperature, inaccurate calculations regarding shade or the fact that the one-diode model with assumed/estimated parameters for ideality factor, R_s and R_p is an approximation and can be slightly off compared to the actual data.

The shaded string without module level dc-dc power optimizers scenario is a representation of how a traditional string would behave. In such a string, a single inverter would control the produced current and voltage for the entire string, leading to every module producing the same amount of power. As visualized in the two figures above, this leads to a significant loss of power. The difference between the MPP of the two shaded scenarios is quite large and represents how much energy could potentially be lost if the system had not been equipped with module level power optimizers.

Table 9: *Power values*

Scenario	**Power**
Power produced by string without shade	888 W
Estimated operational point for the given circumstances	800 W
Power produced with a traditional configuration	354 W
Power lost to shade	88 W
Power potentially lost to shade	533 W
Power reclaimed	445 W

In Table 9 the power produced in the different scenarios simulated above are presented. The estimated operational point is approximately accurate and serves for discussing how the module level DC-DC power optimizers operates. As can be seen from both the table and Figure 23a and 23b is as expected unable to operate at the strings maximum value due to one module being exposed to shade. When comparing it to a hypothetical system without module level DC-DC power optimizers the difference in produced power is quite significant. This difference is what the module level DC-DC power optimizers "reclaim" and would in a system with string inverter MPPT be lost.

4.3 Creating nonuniform operating conditions

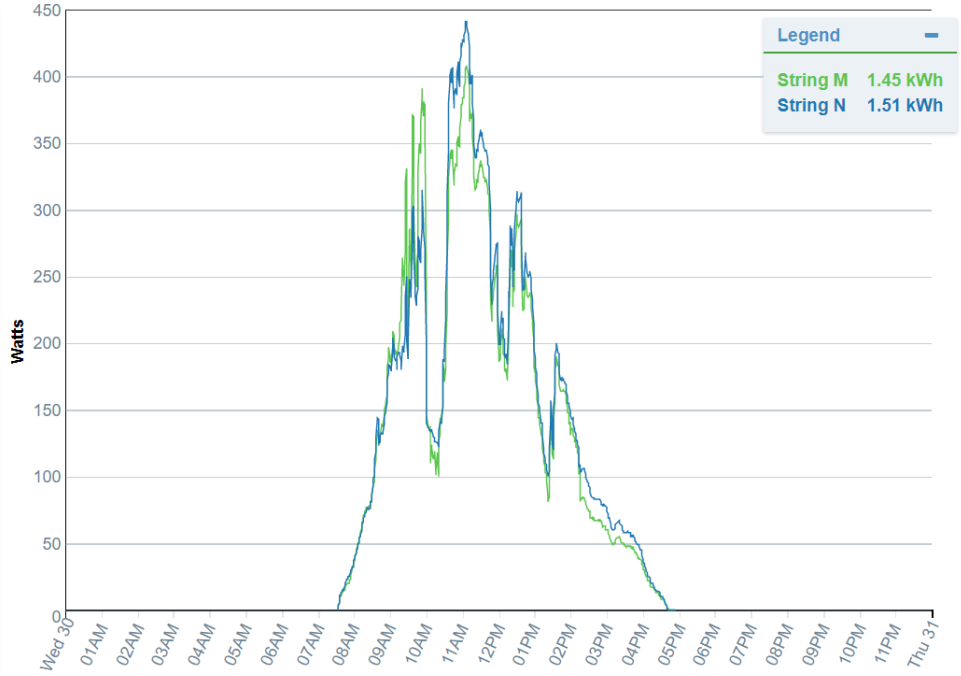

Figure 24: *The energy generated in the course of a day, relating a module that is partially covered and one not covered*

From Figure 24 the produced power in the course of a day from two separate strings are presented. The day in question is the 30.10.2019. String M as mentioned earlier in Section 3.4, has a module covered as in Figure 11. String N is a string with the same orientation and technology, but is neither covered by plastic nor inflicted by shade. It functions therefore as an ideal string to be compared string M to.

By observing Figure 24 it is possible to detect a difference in produced power after a certain time. The difference is not apparent until mid-morning when module M1 was partially covered. Firstly, string M have an higher energy generation than string N. This can be contributed to the covering process, where shade can have been inflicted on string N by people on the roof. After the easily observed dip in power production, string M consequently produces less power than string N. The observed difference after the substring has been covered is not very substantial. As discussed above, when a substring is sufficiently exposed to mismatch conditions that substring is effectively removed from the module causing the module to produce less power. This

is depicted in Figure 25

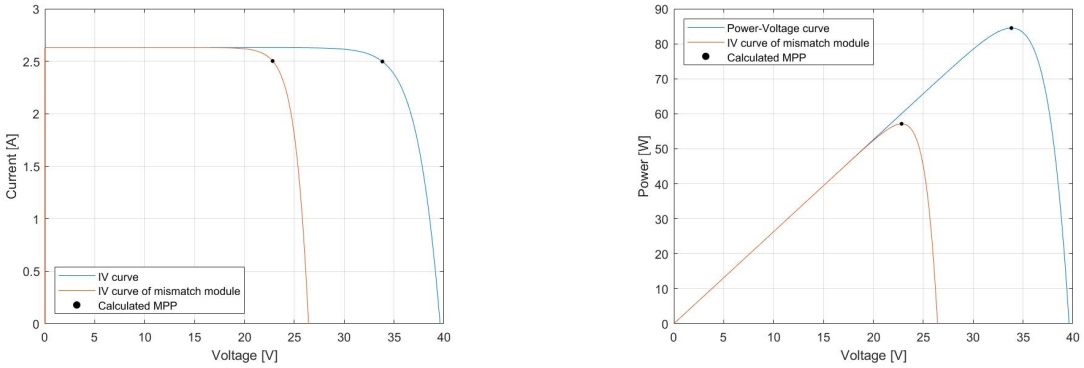

(a) *IV curves* (b) *Power-Voltage curves*

Figure 25: *Curves displaying the effect of having one substring exposed to severe mismatch.*

As can be seen from Figure 25a the current of the calculated MPP is identical, as is the short-circuit current. Since solar cells are connected in series the current through each ccell will be equal, hence the cells part of the substrings that are not covered will produce the same amount of current as if no part of the module was covered at all. However, the voltage will decrease and can easily be detected in Figure 25b. In a series connection the total voltage will increase for each energy source embedded in the system. When 1/3 of the energy sources are removed the voltage will experience a drop of 1/3, as will the power.

The power lost by a single module will affected the total production of the entire string. However, since it is mainly the voltage that is affected in this scenario the produced power by the entire string will not be seriously reduced. This is again due to the strings being series connected where the behaviour of each individual module is dependent upon the current produced by the other modules in the same string. This is displayed in Figure 26.

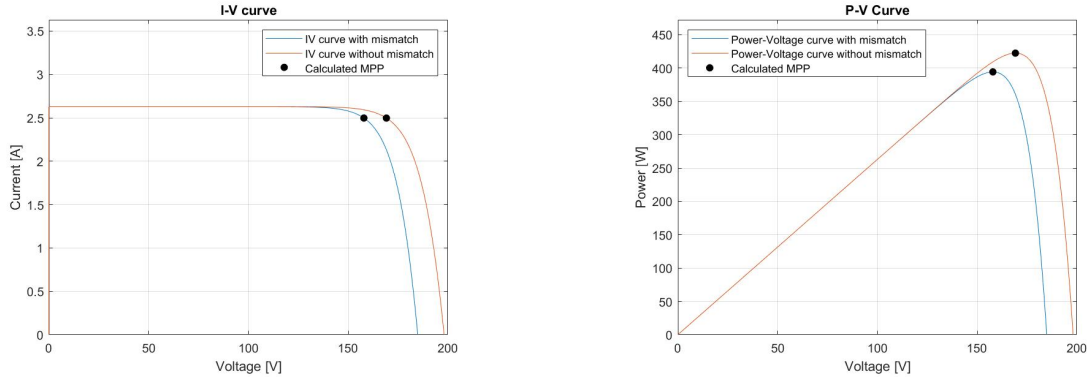

(a) *IV curves* (b) *Power-Voltage curves*

Figure 26: *How a single substring can effect the power produced by an entire string*

Figure 26 demonstrates why the difference in generated energy for string M and N is not bigger. As can be seen the difference between an unimpaired string and an impaired string is due to the voltage of that single module not being as high as for the remaining modules. Due to the voltage of a single module being the parameter mostly affected the power optimizers should have to interfere in order to allow the unaffected modules to operate as normal. That is also the case where Tigo reports that there is virtually no reclaimed energy for string M in the case of this experiment.

The two other modules that where covered were both part of string K. Neither of them was expected to produce power since the Module K5 had parts of all three substrings covered by plastic as in Figure 12 and the entire surface of Module K4 was covered as in Figure 13. Neither does Tigo report that they do. However, none of the three remaining modules are producing as well. Given that the TS4 optimizers should allow each module in a string to perform at its individual maximum power point. Why this does not happen in this scenario is to the author unknown given how the impedance matching supposedly works.

4.4 Shade from fence

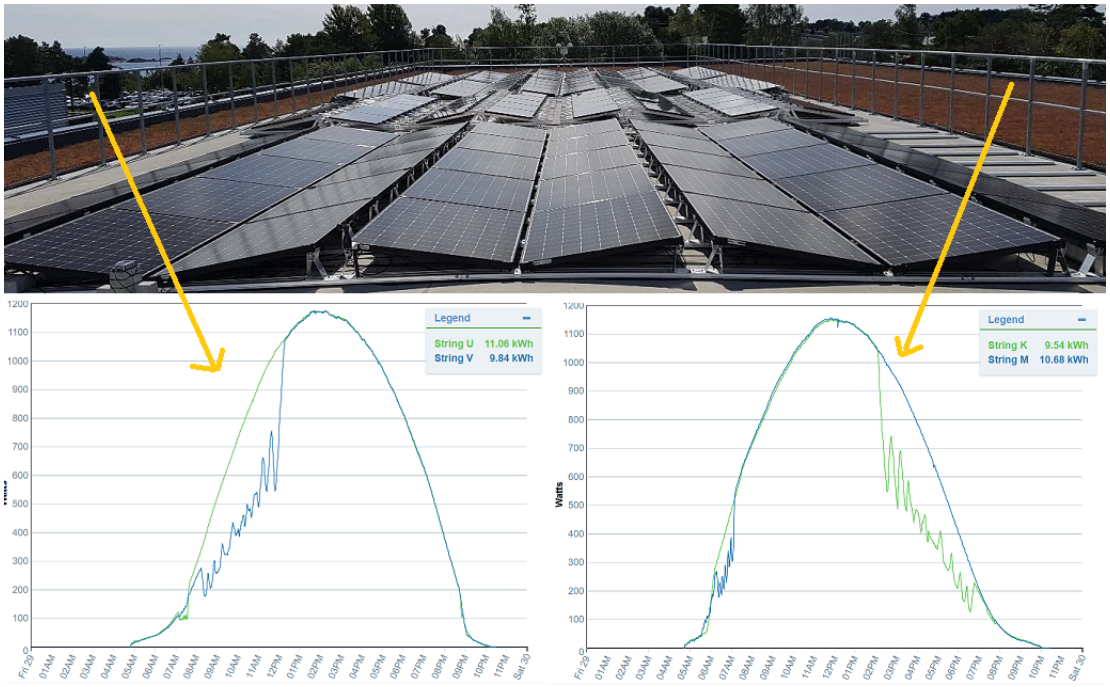

Figure 27: *How the shade from the surrounding fence influences the system*

In Figure 27 the impact the surrounding fence has on the system is displayed. As can be seen the fence impacts different strings at different times of the day. This is due to the apparent motion of the sun. The difference in the energy produced when exposed to shading conditions is quite extensive. However, only the strings in the vicinity of the fence is affected by it, allowing the remaining strings to operate at their maximum potential for the given circumstances. The losses are more severe during the winter than summer. This is due to the sun operating lower on the horizon, thus inflicting more shade on the system.

4.5 Performance

4.5.1 Mono-Si vs poly-Si modules

The specific energy yield of the different PV modules are presented in Table 10

Table 10: *Specific energy yield*

Name	Specific energy for the entire group	Specific energy for a single module
Poly-Si	406 kWh/kW_p	434 kWh/kW_p
Mono-Si	415 kWh/kW_p	422 kWh/kW_p

When considering the specific energy for a single module it is possible to discern that the poly-Si modules outperform the mono-Si modules. This could be related to the previously discussed subjected concerning the ideality factor. The poly-Si modules are seemingly able adopt a much closer behaviour to their ideal potential than the mono-Si modules are.

Both the individual modules have a higher specific energy yield than the entire group of modules. This is due to modules and strings being subjected to shade, causing the groups to have a reduction in energy generation. When inspecting the entire group of modules, the mono-Si modules outperform the poly-Si modules even though the single poly-Si module have a higher specific energy yield than the mono-Si modules. This can be explained by the fact that the mono-Si modules are less exposed to shade than the poly-Si modules are. Had the individual modules not been equipped with power optimizers the difference between the total production of the two technologies would have been more severe.

4.5.2 Total energy production

The total energy produced by the grid connected PV system investigated as of 05.06.2020 is displayed in Table 11.

Table 11: *Total energy produced as reported by Tigo*

Scenario	**Energy**
Total energy produced	38.02 MWh
Energy base	36.96 MWh
Total energy reclaimed	1.06 MWh

As can be seen the total amount of reclaimed energy is quite low. This implies that the system has a low degree of mismatch. As mentioned in a section above, the main contributor to mismatch is the fence. From the amount reclaimed it is possible to discern that it does not have a big influence on the system.

As mentioned in Section 2.5.1 power optimizers could potentially be placed only on modules affected by mismatch conditions. This could potentially greatly decrease the cost of building a new system. However, having the TS4 power optimizers on each module allows for the observation of each module, and subsequently the entire system. This provides a value in itself, as it allows for easy investigation of the system and quick localisation of anything not working as it supposedly should.

5 Conclusion

In regards to the mathematical model it functions reasonably well, and it is able to imitate the behaviour of the system to a certain extent. The choice to use the five parameter model is justified through the various investigated scenarios. The calculated MPP deviates ever so slightly from the actual MPP, but it is within acceptance. There is a slight difference in the behaviour between the Matlab model and the Simulink model where current is concerned rendering it a bit more unaccurate than the Matlab model.

The module level DC-DC power optimizers are able to satisfyingly mitigate mismatch conditions for the investigated situation in Section 4.2. As confirmed by the mathematical model the optimizers are able to allow the modules unaffected by shade in the same string to operate at their individual maximum power point. The power optimizers are also able to not include situations such as the one presented in Figure 11 as reclaimed energy for the remainder of the string as there occurs no considerable mismatch regarding the current, only voltage. However, the optimizers are unable to perform as expected when two modules in a string are so heavily mismatched that they are unable to produce any energy. In such a scenario the remaining modules do not produce energy at all.

The poly-Si modules are able to perform better than the mono-Si modules with respect to their MPP at STC. The poly-Si modules are able to operate clsoer to their ideal value and will therefore operate with a higher sepcific energy yield.

The mismatch present in the system from the fence and pyranometer is not very extensive. It only affects the modules in its vicinity and the optimizers are able to effectively hinder a decline in energy generation for the other modules in the string. When studying the total energy produced by the system a small amount of it is contributed as reclaimed energy. This implies that for the majority of modules having module level DC-DC power optimizers are unnecessary in regards to energy generation, and could have been fitted with a traditional string inverter MPPT. The

modules affected by shade could be equipped with a single optimizers as the PIV technology would allow it to be placed on a single module in a string without affecting the other modules. However, having power optimizers on a module level have their benefits even though they do not necessarily mitigate mismatch. The TS4 optimizers are as previously mentioned able to monitor the energy generation and report values for further investigation. This has value in being able to study the system quite accurately as well as easily detecting faults. Furthermore, as the system becomes older it may experience mismatch from other sources then shade, such as damaged cells or simply deterioration of cells, hence having module level power optimizers would then be desirable.

6 Recommendations for further work

For further investigation of the system several new experiments could be conducted where different shading scenarios are studied. The economics of the system could also be investigated where the cost-benefit of having module level optimizers could be compared against a system with centralized string inverter MPPT.

References

[1] L. Chaar, L. Lamont, and N. Zein. Review of Photovoltaic Technologies. *Renewable and Sustainable Energy Reviews*, 15:2165–2175, 06 2011.

[2] Solar Energy Market Strategies and Forcasts, 2019 to 2026. `https://coleofduty.com/news/2020/06/05/solar-energy-market-strategies-and-forecasts-2019-to-2026/`, June 2020.

[3] Ilham Nassar-Eddine and Obbadi Abdellatif. Parameter Estimation of Photovoltaic Modules Using Iterative Method and the Lambert W Function: A Comparative Study. *Energy Conversion and Management*, July 2016.

[4] Michael J. Brandemuehl, Robert W. Erickson, and Sara M. MacAlpine. Characterization of Power Optimizer Potential to Increase Energy Capture in Photovoltaic Systems Operating Under Nonuniform Conditions. *IEEE Transactions on Power Electronics*, 28(6):2936–2945, June 2013.

[5] Amit Kuder Podder, Hemanshu Roy Pota, and Naruttam Kumar Roy. MPPT Methods for Solar PV System: A Critical Review Based on Tracking Nature. *IET Renewable Power Generation*, April 2019.

[6] Giovanni Celsa and Giuseppe Tina. Matlab/Simulink Model of Photovoltaic Modules/Strings Under Uneven Distribution of Irradiance and Temperature. *2015 6th International Renewable Energy Congress, IREC 2015*, May 2015.

[7] Ole-Kristian Nese. Locating Mismatch Factors and Analyzing the Performance Gain from Module Level Power Optimizers in a PV System. Technical report, University of Agder, 2019.

[8] Richard Corkish, Martin Green, Muriel Watt, and Stuart Wenham. *Applied Photovoltaics*. Earthscan, second edition, 2007.

[9] Steven McFadyen. Photovoltaic - Electric Clalculations. `https://myelectrical.com/notes/entryid/225/photovoltaic-pv-electrical-calculations`, July 2013.

[10] Nominal Operating Cell Temperature. `https://www.pveducation.org/pvcdrom/modules-and-arrays/nominal-operating-cell-temperature`.

[11] Jan Holtet. Pyranometer. https://snl.no/pyranometer, March 2020.

[12] Stuart Bowden and Christina Honsberg. Hot Spot Heating. https://www.pveducation.org/pvcdrom/modules-and-arrays/hot-spot-heating.

[13] Stuart Bowden and Christina Honsberg. Bypass Diodes. https://www.pveducation.org/pvcdrom/modules-and-arrays/bypass-diodes.

[14] Ned Mohan. *Power Electrics; A First Course*. Wiley.

[15] Inverter. https://www.sunpower-uk.com/glossary/what-is-an-inverter/.

[16] Stephen Chapman. *Electrical Machinery Fundamentals*. MacGraw-Hill, 4 edition.

[17] Ralf Muenster. Power Optimizers: Centralized vs Distributed MPPT. https://www.renewableenergyworld.com/2009/09/15/power-optimizers/#gref.

[18] Henrique Braga, Pedro Barbosa, Andre Ferreira, and Fernando Tofoli. Analysis of MPPT Techniques Applied to the DCM Multiphase Boost Converter for the Mitigation of Partial Shading in Pv Arrays. In *Brazilian Power Electronics Conference*, September 2011.

[19] Miguel García, Jose Maruri, Luis Marroyo, Eduardo Pigueiras, and Miguel Perez. Partial Shadowing, MPPT Performance and Inverter Configurations: Observations at Tracking PV Plants. *Progress in Photovoltaics: Research and Application*, April 2008.

[20] Tigo. Maximizing Energy Harvest: The Roles of Predictive IV and Impedance Matching in PV Array Optimization.

[21] C.S. Kong. A General Maximum Power Theorem. *IEEE Transactions on Eductaion*, 38:296–298, August 1995.

[22] Alper Erturk, Daniel Inman, Na Kong, and Dong Sam Ha. Resistive Impedance Matching Circuit for Piezoelectric Energy Harvesting. *Journal of Intelligent Material Systems and Structures*, 21:1293 – 1302, 2010.

[23] Optimization with Predictive IV and Impedance Matching. https://support.tigoenergy.com/hc/en-us/articles/203180067-Optimization-with-Predictive-IV-and-Impedance-Matching.

[24] Tigo. Impedance Matching: The Science Behind the Tigo Optimizer, February 2013.

[25] Habbati Bellia, Moulay Fatima, and Ramdani Youcef. A Detailed Modeling of a Photovoltaic Module Using Matlab. *NRIAG Journal of Astronomy and Geophysics*, May 2014.

[26] Khomdram Jolson Singh, Kristen Kho, Sapam Jitu Singh, Yengkhom Chandrika Devi, Nameirakpam Basanta Singh, and Subir Kumar Sarkar. Artificial Neural Network Approach for More Accurate Solar Cell Electrical Circuit Model. *International Journal of Computer Science and Applications*, 4:101–116, 2014.

[27] Marcelo Villalva, Jonas Gazoli, and Ernesto Filho. Comprehensive Approach to Modeling and Simulation of Photovoltaic Arrays. *Power Electronics, IEEE Transactions on*, 24:1198 – 1208, 06 2009.

[28] Stefano Bifaretti, Armando Bellini, Cristina Cornaro, and Vincenzo Iacovone. Simple Model of a Photovoltaic System. In *Proceedings of the IEEE Applied Electronics*.

[29] Christopher A. Deline, Alex J. Hanson, Sarah M. MacAlpine, Jason T. Stauth, and Charles R. Sullivan. Partial-Shading Assesment of Photovoltaic Installations via Module-Level Monitoring. *IEEE Journal of Photovoltaics*, 4(6):396–404, November 2014.

[30] Chris Deline, Sigifredo Gonzales, Jennifer Granata, and Bill. Marion. A Performance and Economic Analysis of Distributed Power Electronics in Photovoltaic Systems. Technical report, National Renewable Energy Laboratory, January 2011.

[31] Chris Deline, Dragan Maksimovic, and Carlos Olalla. Perfromance of Mismatched PV Systems with Submodule Integrated Converters. *IEEE Journal of Photovoltaics*, 4(1):396–404, January 2014.

[32] Pengju Kong, Fred C. Lee, Feng Wang, Zijian Wang, Xinke Wu, and Fang. Zhuo. Analysis of Unified Output MPPT Control in Subpanel PV Converter System. *IEEE Transactions on Power Electronics*, 28(6):2936–2945, June 2013.

[33] P. Tsao. Simulation of PV Systems with Power Optimizers and Distributed Power Electronics. In *2010 35th IEEE Photovoltaic Specialists Conference*, pages 000389–000393, June 2010.

[34] Massimiliano De Cristofaro, Giulia Di Capua, N. Femia, Giovanni Petrone, Giovanni Spagnuolo, and Davide Toledo. Models and Methods for Energy Productivity Analysis of PV Systems. Technical report, University of Salerno, 07 2015.

Appendices

A Extra figures

A.1 Modelling of diode current

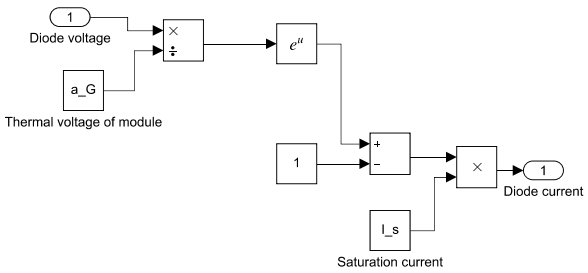

Figure 28: *The various components used to calculate the diode current in Simulink*

B Code

B.1 Determining R_p and R_s

B.1.1 Mono

```
clc; close all; clear;
%Locating Rp and Rs
%% Given values
P_mpp=315; % [W]
I_mpp=9.53; I_sc=10.02; % [A]
V_mpp=33.1; V_oc=40.5; % [V]
N_s=60;
%% STC
G_stc=1000; %[W/m^2]
T_stc=25; %[C^o]
%% Set values and constants
A=1.2; %Ideality factor
q=1.6021e-19; %Elementary charge [C]
k=1.3805e-23; %Boltzman constant [J/K]
e_g=1.12; %band gap for silicon
T_abs_conv=273; %conversion from Celsius to Kelvin [K]
T_c=25; %Cell temperature in Celsius
T_c_abs=T_c+T_abs_conv;
T_stc_abs=T_stc+T_abs_conv;
alpha=0.0013; %Temperature coefficient of current
G=1000;
%% Calculated values
V_t=k*T_c_abs/q; %Thermal voltage [V]
a=N_s*A*V_t; %Thermal voltage when considering number of cells and
    ideality factor %[V]
R_p_ini=V_mpp/(I_sc-I_mpp)-(V_oc-V_mpp)/I_mpp; %initial value of
    parallel resistance[ohm]
%% Iterate
tolerance=1e-2;
I_ph=I_sc; %Photocurrent [A]
I_s=I_sc/(exp(V_oc/a)-1); %Saturation current [A]
%Loop
V=0; %Initial value
c=1; %Counter
h=1e-4; %Step size
R_s=0; % initial value of series resistance [ohm]
I_n_guess=1.5; %Initial guess at current
```

```
%Locating current, voltage and power values with the Newton-Raphson
   method
while V<V_oc
   c=c+1;
   for i=10
       if V==0
           I_n=I_sc;
       else
           I_n=I_sc-I_s*(exp((V+R_s*I_n1)/a)-1)-(V-R_s*I_n1)/R_p_ini;
               %Newton-Raphson
       end
   I_n1=I_n-(I_sc-I_n-I_s*(exp((V+I_n*R_s)/a)-1))/(-1-I_s*R_s/a*(exp
      ((V+I_n*R_s)/a)-1)); %Newton-Raphson
   end
   P=V*I_n1;
   V=V+h;
   Pp(c)=P;
   Ii(c)=I_n1;
   Vv(c)=V;
end
figure
plot(Vv,Ii)
hold on
yyaxis right
plot(Vv,Pp)
grid;
P_max=max(Pp);
error=abs(P_mpp-P_max);
%New calc
VN=0;
R_s_e=error/90.05; %New value of series resistor
%R_s_e=0;
R_p_e=V_mpp*(V_mpp+I_mpp*R_s_e)/(V_mpp*I_ph-V_mpp*I_s*exp((V_mpp+
   I_mpp*I_s)/a)+V_mpp*I_s-P_mpp); %New value of parallel resistor
%R_p_e=(V_mpp+I_mpp*R_s_e)/(I_sc-I_sc*exp((V_mpp+R_s_e*I_mpp-V_oc)/a)
   +I_sc*exp(-V_oc/a)-P_mpp/V_mpp);
I_pv_n=I_sc*(R_s_e+R_p_e)/R_p_e;
```

```
%Locating current, voltage and power values by the use of Newton-Raphson
while VN<V_oc
    c=c+1;
    for i=10
        if VN==0
            I_N=I_sc;
        else
            I_N=I_ph-I_s*(exp((VN+R_s_e*I_N1)/a)-1)-(VN-R_s_e*I_N1)/R_p_e; %[A]
        end
    I_N1=I_N-(I_ph-I_N-I_s*(exp((VN+I_N*R_s_e)/a)-1))/(-1-I_s*R_s_e/a*(exp((VN+I_N*R_s_e)/a)-1)); %[A]
    end
    P_N=I_N1*VN; %[W]
    PP(c)=P_N;
    II(c)=I_N1;
    VV(c)=VN;
    VN=VN+h;
    %R_s_e=R_s_e+h;
end
PN_max=max(PP); %[W]
err=abs(P_mpp-PN_max);
figure
plot(VV,II)
hold on
yyaxis right
plot(VV,PP)
grid;
```

B.1.2 Poly

```
clc; close all; clear;
%Locating Rp and Rs for poly
%% Given values
P_mpp=270; % [W]
I_mpp=8.50; I_sc=9.08; % [A]
V_mpp=31.7; V_oc=38.9; % [V]
```

```
N_s=60
gamma=-0.417; % Temperature coefficient at stc for Pmp [%/K]
alpha=0.037; % Temperature coefficient at stc for Isc [%/K]
beta=-0.13; % Temperature coefficient at stc for Voc [V/K]
%% STC
G_stc=1000; %[W/m^2]
T_stc=25; %[C^o]
%% Set values and constants
q=1.6021e-19; %Elementary charge [C]
k=1.3805e-23; %Boltzman constant [J/K]
e_g=1.12; %band gap for silicon
T_abs_conv=273; %conversion from Celsius to Kelvin [K]
T_c=25; %Cell temperature in Celsius
T_c_abs=T_c+T_abs_conv; %Cell temperature in Kelvin
T_stc_abs=T_stc+T_abs_conv; %STC in Kelvin
alpha=0.0013; %Temperature coefficient of current [1/K]
beta=-0.13; %[V/K]
G=1000; %Irradiance at STC [W/m^2]
%% Calculated values
V_t=k*T_c_abs/q; %Thermal voltage [V]
%A=1.3; %Ideality factor
A=(beta-V_oc/T_stc_abs)/(N_s*V_t*(alpha/(100)-3/T_stc_abs-e_g*q/(k*
    T_stc_abs^2)));
a=N_s*A*V_t; %Thermal voltage when considering number of cells and
    ideality factor %[V]
R_p_ini=V_mpp/(I_sc-I_mpp)-(V_oc-V_mpp)/I_mpp; %initial value of
    parallel resistance[ohm]
%% Iterate
tolerance=1e-2;
%I_ph=G/G_stc*(I_sc+alpha*(T_c-T_stc)); %Photocurrent
I_ph=I_sc; %Photocurrent [A]
I_s=I_sc/(exp(V_oc/a)-1); %Saturation current [A]
%Loop
V=0; %Initial value
c=1; %Counter
h=1e-4;
R_s=0; % initial value of series resistance [ohm]
I_n_guess=1.5;
```

```
%Locating current, voltage and power values with the Newton-Raphson method
 while V<V_oc
    c=c+1;
    for i=10
        if V==0
            I_n=I_sc-I_s*(exp((V+R_s*I_n_guess)/a)-1)-(V-R_s*I_n_guess)/R_p_ini;
        else
            I_n=I_sc-I_s*(exp((V+R_s*I_n1)/a)-1)-(V-R_s*I_n1)/R_p_ini;
        end
    I_n1=I_n-(I_sc-I_n-I_s*(exp((V+I_n*R_s)/a)-1))/(-1-I_s*R_s/a*(exp((V+I_n*R_s)/a)-1));
    end
    P=V*I_n1;
    V=V+h;
    Pp(c)=P;
    Ii(c)=I_n1;
    Vv(c)=V;
 end
 figure
 plot(Vv,Ii)
 hold on
 yyaxis right
 plot(Vv,Pp)
 grid;
 P_max=max(Pp);
 error=abs(P_mpp-P_max);
 %New calc
%R_s_e=error/90.05;
R_s_e=error/95.8;
 VN=0;
 R_p_e=V_mpp*(V_mpp+I_mpp*R_s_e)/(V_mpp*I_ph-V_mpp*I_s*exp((V_mpp+I_mpp*I_s)/a)+V_mpp*I_s-P_mpp);
 %R_p_e=(V_mpp+I_mpp*R_s_e)/(I_sc-I_sc*exp((V_mpp+R_s_e*I_mpp-V_oc)/a)+I_sc*exp(-V_oc/a)-P_mpp/V_mpp);
 I_pv_n=I_sc*(R_s_e+R_p_e)/R_p_e;
```

```
74  %Locating current, voltage and power values with the Newton-Raphson
        method
75  while VN<V_oc
76      c=c+1;
77      for i=10
78          if VN==0
79              I_N=I_sc;
80          else
81              I_N=I_ph-I_s*(exp((VN+R_s_e*I_N1)/a)-1)-(VN-R_s_e*I_N1)/
                    R_p_e;
82          end
83      I_N1=I_N-(I_ph-I_N-I_s*(exp((VN+I_N*R_s_e)/a)-1))/(-1-I_s*R_s_e/a
            *(exp((VN+I_N*R_s_e)/a)-1));
84      end
85      P_N=I_N1*VN;
86      PP(c)=P_N;
87      II(c)=I_N1;
88      VV(c)=VN;
89      VN=VN+h;
90      %R_s_e=R_s_e+h;
91  end
92  %  R_s_e=R_s_e+h;
93  PN_max=max(PP); [true_pn, row_pn]=ismember(PN_max,PP,'legacy');
94  V_max=VV(row_pn); I_max=II(row_pn);
95  err=abs(P_mpp-PN_max);
96  figure
97  plot(VV,II)
98  hold on
99  yyaxis right
100 plot(VV,PP)
101 grid;
```

B.2 Determinig operating parameters for actual data

B.2.1 Mono

```
1  clc; close all; clear;
2  %Mathematical model with five parameter method
```

```
%n significe STC
%% Given values
P_mpp=315; % [W]
I_mpp=9.53; I_sc_stc=10.02; % [A]
V_mpp=33.1; V_oc_stc=40.5; % [V]
N_s=60;
V_mpp_sh=33.1*2/3; V_oc_sh=40.5*2/3; %Voltage for experiment [V]
N_s_sh=40; %Number of cells producing power in experiment
gamma=-0.38; % Temperature coefficient at stc for Pmp [%/K]
alpha=0.06; % Temperature coefficient at stc for Isc [%/K]
beta=-0.1134; % Temperature coefficient at stc for Voc [V/K]
NOCT=44; %Nominal Operating Cell Temperature [Celsius]
G_noct=800; %[W/m^2]
%% STC
G_stc=1000; %[W/m^2]
T_stc=25; %[C^o]
%% Set values and constants
q=1.6021e-19; %Elementary charge [C]
k=1.3805e-23; %Boltzman constant [J/K]
e_g=1.12; %band gap for silicon
T_abs_conv=273; %conversion from Celsius to Kelvin [K]
T_c=25; %Cell temperature in Celsius
G=1000; % [W/m^2]
%% Loaded data
%Weather_data_may=importdata('WeatherMai.xlsx'); %irr,temp, etc on a
    per minute base
Weather_data=importdata('Weather_feb_mar.csv');  %irr, temp, etc on a
    per minute base
%Tigo_data_M1=importdata('Tigo_110320_M1.csv'); %data downloaded from
    Tigo [W]
%Weather_data_oct=importdata('Weather_Okt.xlsx');
%% String data
%M
P_M1=87; P_M2=56; P_M3=88; P_M4=88; P_M5=165; % [W]
P_tigo=P_M1+P_M2+P_M3+P_M4+P_M5;
I_M1=2.64; I_M2=2.43; I_M3=2.59; I_M4=2.59; I_M5=5;% [A]
V_M1=33; V_M2=23; V_M3=34; V_M4=34; V_M5=33; %[V]
V_tigo=V_M1+V_M2+V_M3+V_M4+V_M5;
```

```
%% Weather
%G_tilt_may=Weather_data_may.data(25922:27360,16);
G_tilt_mar=Weather_data.data(43200:44639,13); %[W/m^2]
%G_tilt_oct=Weather_data_oct.data(1439:2878,14); %[W/m^2]
G_max=max(G_tilt_mar); [true_irr, row_irr]=ismember(G_max,G_tilt_mar,'row');
%G_max=max(G_tilt_may); [true_irr, row_irr]=ismember(G_max,G_tilt_may,'row');
%G_max=max(G_tilt_oct); [true_irr, row_irr]=ismember(G_max,G_tilt_oct,'row');
T_amb_mar=Weather_data.data(43200:44639,31); %Ambiant temperature [C]
%T_amb_may=Weather_data_may.data(25922:27360,33);
%T_amb_oct=Weather_data_oct.data(1439:2878,34);
%T_amb_op=T_amb_oct(row_irr);
%% Temperature
T_op=T_amb_mar+(NOCT-20)*G_tilt_mar/G_noct; %Celsius
T_op_G=T_op(row_irr);  %Celsius
deltaT=T_op_G-T_stc; % Celsius
T_op_abs=T_op_G+T_abs_conv; %Kelvin
T_c_abs=T_c+T_abs_conv; %Kelvin
T_stc_abs=T_stc+T_abs_conv; %Kelvin
V_t_G=k*(T_op_abs)/q; %Thermal voltage [V]
%% Calculated values
A=1.2; %Ideality factor for mono crystalline cells
%A=(beta-V_oc_stc/T_stc_abs)/(N_s*V_t*(alpha/(100)-3/T_stc_abs-e_g*q/(k*T_stc_abs^2)));
a_G=N_s*A*V_t_G; %Thermal voltage when considering number of cells and ideality factor [V]
a_sh=N_s_sh*A*V_t_G;
V_t=k*T_c_abs/q; %Thermal voltage [V]
a=N_s*A*V_t; %Thermal voltage when considering number of cells and ideality factor [V]
R_p=109.2119; %[ohm]
R_s=0.1976; %[ohm]
%% IV
%Five parameter model
I_sc=I_sc_stc*(1+alpha*(T_stc-T_op_G)/100); %Actual short-circuit voltage [A]
```

```
I_pv_n=(R_s+R_p)/R_p*I_sc_stc; %Photocurrent at STC [A]
I_s_n=I_sc_stc*(1+R_s/R_p)/(exp(V_oc_stc/a_G)-1);
I_pv=G_max/G_stc*I_sc*(1+alpha*(T_stc-T_op_G)/100); %Actual
    photocurrent [A]
I_s=(I_sc_stc+alpha*(T_stc-T_op_G)/100+(R_s*(I_sc_stc+alpha*(T_stc-
    T_op_G)/100)-V_oc_stc-beta*(T_op_G-T_stc))/R_p)/exp((V_oc_stc+beta
    *(T_op_G-T_stc))/a_G); %Actual saturation current [A]
V_oc=a_G*log(I_pv_n/I_s_n+1); %[V]
V_oc_G=V_oc_stc+beta*(T_c-T_op_G)+a_G*log(G_max/G_stc); %[V]
V=0;
c=1;
h=1e-4;
%Locating current, voltage and power values with the Newton-Raphson
    method
while V<V_oc
     c=c+1;
     for i=10
         if V==0
             I_n=I_sc;
         else
             I_n=I_pv-I_s*(exp((V+R_s*I_n1)/a_G)-1)-(V-R_s*I_n1)/R_p;
         end
     I_n1=I_n-(I_pv-I_n-I_s*(exp((V+I_n*R_s)/a_G)-1))/(-1-I_s*R_s/a_G
        *(exp((V+I_n*R_s)/a_G)-1));
     end
     if I_n1<=0
         break
     end
     P=I_n1*V;
     PPlot(c)=P;
     IPlot(c)=I_n1;
     VPlot(c)=V;
     V=V+h;
end
% Shaded scenario with the five parmameter model
I_pv_sh=G_max/G_stc*I_sc*(1+alpha*(T_stc-T_op_G)/100); %Actual
    photocurrent [A]
```

```
I_s_sh=(I_sc_stc+alpha*(T_stc-T_op_G)/100+(R_s*(I_sc_stc+alpha*(T_stc-
    T_op_G)/100)-V_oc_stc-beta*(T_op_G-T_stc))/R_p)/exp((V_oc_stc+beta
    *(T_op_G-T_stc))/a_G);
V_sh=0;
%Locating current, voltage and power values with the Newton-Raphson
    method
while V_sh<V_oc_sh
     c=c+1;
     for i=10
         if V_sh==0
             I_n_sh=I_sc;
         else
             I_n_sh=I_pv_sh-I_s_sh*(exp((V_sh+R_s*I_n1_sh)/a_sh)-1)-(
                 V_sh-R_s*I_n1_sh)/R_p;
         end
     I_n1_sh=I_n_sh-(I_pv_sh-I_n_sh-I_s_sh*(exp((V_sh+I_n*R_s)/a_sh)
        -1))/(-1-I_s_sh*R_s/a_sh*(exp((V_sh+I_n_sh*R_s)/a_sh)-1));
     end
     if I_n1_sh<=0
         break
     end
     P_sh=I_n1_sh*V_sh;
     P_shPlot(c)=P_sh;
     I_shPlot(c)=I_n1_sh;
     V_shPlot(c)=V_sh;
     V_sh=V_sh+h;
end
%locating MPP
P_max_5=max(PPlot); [true_5, column_5]=ismember(P_max_5,PPlot,'legacy'
    );
V_5=VPlot(column_5);
I_5=IPlot(column_5);
P_max_sh=max(P_shPlot); [true_sh, column_sh]=ismember(P_max_sh,
    P_shPlot,'legacy');
V_5_sh=V_shPlot(column_sh);
I_5_sh=I_shPlot(column_sh);
%err=abs(P_mpp-P_max_5);
%Simplified model
```

```
It_1000=I_sc*G_max/G_stc; %Short circuit current based on irradiance
    alone [A]
Isc_1000=It_1000*(1+alpha*(T_stc-T_op_G)/100); %Calculated Isc based
    on irradiance and temperature [A]
Imp_1000=I_mpp*G_max/G_stc*(1+alpha*(T_stc-T_op_G)/100); %Calculated
    Imp based on irradiance and temperature [A]
Voc_m_ini=30; %Initial guess at open-circuit voltage [V]
V_1000=0;
h=1e-4; %Step
c=1; %Counter
for i=1:8
    if i==1
        Voc_m_1000=Voc_m_ini;
    else
        Voc_m_1000=Voc_m_iterate_1000;
    end
    deltaV_1000=V_oc-Voc_m_1000;
    Voc_1000=V_oc+beta*(T_op_G-T_stc)-deltaV_1000; %Calculated  open
       circuit voltage based on temperature [V]
    Vmp_1000=V_mpp+beta*(T_op_G-T_stc)-deltaV_1000; %Calculated Vmp
       based on temperature [V]
    C_2_1000=(Vmp_1000/Voc_1000-1)/log(1-Imp_1000/Isc_1000);
    C_1_1000=(1-Imp_1000/Isc_1000)*exp(-Vmp_1000/(C_2_1000*Voc_1000));
    Voc_m_iterate_1000=C_2_1000*V_oc*log(1+(It_1000/I_sc)/C_1_1000);
end
while V_1000<Voc_1000
    V_1000=V_1000+h;
    c=c+1;
    I_1000=Isc_1000*(1-C_1_1000*(exp(V_1000/(C_2_1000*Voc_1000))-1));
    P_1000=I_1000*V_1000;
    P_1000Plot(c)=P_1000;
    I_1000Plot(c)=I_1000;
    V_1000Plot(c)=V_1000;
    if I_1000<=0
        break
    end
end
P_max_simple=max(P_1000Plot); %[W]
```

```
164 [true_simple, column_simple]=ismember(P_max_simple,P_1000Plot,'legacy'
    );
165 V_mpp_simple=V_1000Plot(column_simple); I_mpp_simple=I_1000Plot(
    column_simple);
166 %% Plot
167 sz=10; %size of calc MPP
168 figure
169 plot(VPlot,IPlot)
170 hold on
171 plot(V_1000Plot,I_1000Plot)
172 scatter(V_M5,I_M5,'filled')
173 scatter(V_mpp_simple,I_mpp_simple,sz,'k','filled')
174 scatter(V_5,I_5,sz,'k','filled')
175 xlabel('Voltage [V]')
176 ylabel('Current [A]')
177 legend('Single diode model','Simplified Model','IBC mono operational
    point','Location','west')
178 grid;
179 figure
180 plot(VPlot,PPlot)
181 hold on
182 plot(V_1000Plot,P_1000Plot)
183 scatter(V_M5,P_M5,'filled')
184 scatter(V_mpp_simple,P_max_simple,sz,'k','filled')
185 scatter(V_5,P_max_5,sz,'k','filled')
186 xlabel('Voltage [V]')
187 ylabel('Power [W]')
188 legend('Single diode model','Simplified model','IBC mono operational
    point','Location','northwest')
189 grid;
190 figure
191 plot(VPlot,IPlot)
192 hold on
193 plot(V_shPlot,I_shPlot)
194 scatter(V_5,I_5,sz,'k','filled')
195 scatter(V_5_sh,I_5_sh,sz,'k','filled')
196 legend('IV curve','IV curve of mismatch module','Calculated MPP','
    location','southwest')
```

```
197 xlabel('Voltage [V]')
198 ylabel('Current [A]')
199 grid;
200 figure
201 plot(VPlot,PPlot)
202 hold on
203 plot(V_shPlot,P_shPlot)
204 scatter(V_5,P_max_5,sz,'k','filled')
205 scatter(V_5_sh,P_max_sh,sz,'k','filled')
206 xlabel('Voltage [V]')
207 ylabel('Power [W]')
208 legend('Power–Voltage curve','IV curve of mismatch module','Calculated
        MPP','location','northwest')
209 grid;
210 %% From Simulink
211 % I_sim=out.Current.Data; %Current from simulink [A]
212 V_string=VPlot*5; %Total voltage for a string [V]
213 V_string_sh=VPlot*4+V_Plot*2/3; %Total voltage for string in
        experiment [V]
214 % V_sim=out.Volt.Data; %Voltage from Simulink [V]
215 % P_sim=I_sim.*V_sim; P_sim_max=max(P_sim); [true_sim, row_sim]=
        ismember(P_sim_max,P_sim,'row');
216 P_string=V_string.*IPlot; P_string_max=max(P_string); [true_string,
        row_string]=ismember(P_string_max,P_string,'legacy');
217 P_string_sh=V_string_sh.*IPlot; P_string_max_sh=max(P_string_sh); [
        true_string_sh, row_string_sh]=ismember(P_string_max_sh,
        P_string_sh,'legacy');
218 %I_sim_max=I_sim(row_sim);
219 I_string_mpp=IPlot(row_string);
220 %V_sim_max=V_sim(row_sim);
221 V_string_mpp=V_string(row_string); V_sh_mpp=V_string_sh(row_string_sh)
        ;
222 %Plot
223 figure
224 plot(V_string_sh,IPlot)
225 hold on
226 plot(V_string,IPlot)
227 %scatter(V_tigo,I_M5,'filled')
```

```
%scatter(V_sim_max,I_sim_max,'k','filled')
scatter(V_string_mpp,I_string_mpp,'k','filled')
scatter(V_sh_mpp,I_string_mpp,'k','filled')
legend('IV curve with mismatch','IV curve without mismatch','
    Calculated MPP')
xlabel('Voltage [V]')
ylabel('Current [A]')
ylim([0 I_pv+1])
title('I-V curve')
grid;
figure
plot(V_string_sh,P_string_sh)
hold on
plot(V_string,P_string)
scatter(V_sh_mpp,P_string_max_sh,'k','filled')
scatter(V_string_mpp,P_string_max,'k','filled')
xlabel('Voltage [V]')
ylabel('Power [W]')
ylim([0 P_string_max+50])
legend('Power-Voltage curve with mismatch','Power-Voltage curve
    without mismatch','Calculated MPP','location','northwest')
title('P-V Curve')
grid;
```

B.2.2 Poly

```
clc; close all; clear;
%Mathematical model with five parameter method
%% Given values
P_mpp=270; % [W]
I_mpp=8.50; I_sc_stc=9.08; % [A]
V_mpp=31.7; V_oc_stc=38.9; % [V]
N_s=60; %Number of cells
gamma=-0.417; % Temperature coefficient at stc for Pmp [%/K]
alpha=0.037; % Temperature coefficient at stc for Isc [%/K]
beta=-0.13; % Temperature coefficient at stc for Voc [V/K]
NOCT=44; %Nominal Operating Cell Temperature [Celsius]
G_noct=800; %[W/m^2]
```

```
%% STC
G_stc=1000; %[W/m^2]
T_stc=25; %[C^o]
%% Set values and constants
q=1.6021e-19; %Elementary charge [C]
k=1.3805e-23; %Boltzman constant [J/K]
e_g=1.12; %band gap for silicon
T_abs_conv=273; %conversion from Celsius to Kelvin [K]
T_c=25; %Cell temperature in Celsius
G=1000;
%% Loaded data
Weather_data_may=importdata('WeatherMai.xlsx'); %irr,temp, etc on a
    per minute base
Weather_data_mar=importdata('Weather_feb_mar.csv');  %irr, temp, etc
    on a per minute base
%C_string=importdata('250520_C_String.csv'); %data downloaded from
C_string=importdata('110320_C_String.csv'); %data downloaded from Tigo
     [W]
%% Individual modules 110320
C_1=C_string.data(:,1);
C_2=C_string.data(:,2);
C_3=C_string.data(:,3);
C_4=C_string.data(:,4);
C_5=C_string.data(:,6);
C_6=C_string.data(:,5);
t_halla=datetime(C_string.textdata(2:end,1),'Format','HH:mm');
%% Shading Index
C_3_max=max(C_3); [true_3, row_3]=ismember(C_3_max,C_3,'row');
C_6_SI=C_6(row_3);
SI_C_6=C_6_SI/C_3_max;
C_1_max=C_1(row_3); C_2_max=C_2(row_3); C_4_max=C_4(row_3); C_5_max=
    C_5(row_3);
P_string_C_max=C_1_max+C_2_max+C_3_max+C_4_max+C_5_max+C_6_SI;
%V_tigo=196; I_tigo=4.142;
P_C6_string=C_6_SI*6;
%% Weather
G_tilt_may=Weather_data_may.data(34559:35998,16);
G_tilt_mar=Weather_data_mar.data(43200:44639,13); %[W/m^2]
```

```
47 %G_max=max(G_tilt_may); [true_irr, row_irr]=ismember(G_max,G_tilt_may
       ,'row');
48 G_max=max(G_tilt_mar); [true_irr, row_irr]=ismember(G_max,G_tilt_mar,'
       row');
49 %G_tilt_west=Weather_data.data(5:end,15); %[W/m^2]
50 t_weather_mar=datetime(Weather_data_mar.textdata(43201:44640,1)); %[
       min]
51 %v_wind=Weather_data.data(43200:44639,26); % average wind speed per
       minute [m/s]
52 T_amb_mar=(Weather_data_mar.data(43200:44639,31)); %Ambiant
       temperature [C]
53 T_amb_may=(Weather_data_may.data(34559:35998,33));
54 T_pv=Weather_data_may.data(8639:10078,22);
55 %% Temperature
56 %T=T_amb_mar(row_irr); disp(T);
57 T_op=T_amb_mar+(NOCT-20)*G_tilt_mar/G_noct; %degrees C
58 T_op_G=T_op(row_irr); %19.77; T_pv(row_irr);
59 deltaT=T_op_G-T_stc;
60 T_c_abs=T_c+T_abs_conv;
61 T_stc_abs=T_stc+T_abs_conv;
62 T_op_abs=T_op_G+T_abs_conv;
63 %% Calculated values
64 V_t_stc=k*T_stc_abs/q;
65 V_t_G=k*(T_op_abs)/q; %Thermal voltage [V]
66 V_t=k*T_c_abs/q; %Thermal voltage [V]
67 A=(beta-V_oc_stc/T_stc_abs)/(N_s*V_t*(alpha/(100)-3/T_stc_abs-e_g*q/(k
       *T_stc_abs^2)));
68 %A=1.3; %Ideality factor for poly crystalline cells
69 a_G=N_s*A*V_t_G; %Thermal voltage when considering number of cells and
        ideality factor [V]
70 a=N_s*A*V_t; %Thermal voltage when considering number of cells and
       ideality factor %[V]
71 R_p=76.602;
72 R_s=0.2331;
73 %% Ideality
74 %% IV
75 %Five parameter model
```

```
I_sc=I_sc_stc*(1+alpha*(T_stc-T_op_G)/100); %Actual short-circuit
    voltage [A]
I_pv_n=(R_s+R_p)/R_p*I_sc_stc; %Photocurrent at STC [A]
I_pv=G_max/G_stc*I_sc*(1+alpha*(T_stc-T_op_G)/100); %Actual
    photocurrent [A]
I_s_n=I_sc_stc*(1+R_s/R_p)/(exp(V_oc_stc/a_G)-1);
%I_s=I_s_n*(T_op_abs/T_c_abs)^3*exp(q*e_g/(A*k)*(1/T_stc_abs-1/
    T_op_abs));
I_s=(I_sc_stc+alpha*(T_stc-T_op_G)/100+(R_s*(I_sc_stc+alpha*(T_stc-
    T_op_G)/100)-V_oc_stc-beta*(T_op_G-T_stc))/R_p)/exp((V_oc_stc+beta
    *(T_op_G-T_stc))/a_G);
V_oc=a_G*log(I_pv_n/I_s_n+1);
V_oc_G=V_oc_stc+beta*(T_c-T_op_G)+a_G*log(G_max/G_stc);
V=0;
c=1;
h=1e-4;
%Locating current, voltage and power values with the Newton-Raphson
    method
while V<V_oc_stc
     c=c+1;
     for i=10
         if V==0
             I_n=I_sc;
         else
             I_n=I_pv-I_s*(exp((V+R_s*I_n1)/a_G)-1)-(V-R_s*I_n1)/R_p;
         end
     I_n1=I_n-(I_pv-I_n-I_s*(exp((V+I_n*R_s)/a_G)-1))/(-1-I_s*R_s/a_G
        *(exp((V+I_n*R_s)/a_G)-1));
     end
     if I_n1<=0
         break
     end
     P=I_n1*V;
     PPlot(c)=P;
     IPlot(c)=I_n1;
     VPlot(c)=V;
     V=V+h;
end
```

```
P_max_5=max(PPlot); [true_5, column_5]=ismember(P_max_5,PPlot,'legacy'
    );
P_try=59.25; [true_try, column_try]=ismember(P_try,PPlot,'legacy'); %
    P_max_5*SI_C_6;
V_5=VPlot(column_5);
I_5=IPlot(column_5);
%Simplified model
It_1000=I_sc*G_max/G_stc; %Short circuit current based on irradiance
    alone [A]
Isc_1000=It_1000*(1+alpha*(T_stc-T_op_G)/100); %Calculated Isc based
    on irradiance and temperature [A]
Imp_1000=I_mpp*G_max/G_stc*(1+alpha*(T_stc-T_op_G)/100); %Calculated
    Imp based on irradiance and temperature [A]
Voc_m_ini=30; %Initial guess at open-circuit voltage [V]
V_1000=0;
h=1e-4; %Step
c=1; %Counter
for i=1:8
    if i==1
        Voc_m_1000=Voc_m_ini;
    else
        Voc_m_1000=Voc_m_iterate_1000;
    end
    deltaV_1000=V_oc-Voc_m_1000;
    Voc_1000=V_oc+beta*(T_op_G-T_stc)-deltaV_1000; %Calculated  open
        circuit voltage based on temperature [V]
    Vmp_1000=V_mpp+beta*(T_op_G-T_stc)-deltaV_1000; %Calculated Vmp
        based on temperature [V]
    C_2_1000=(Vmp_1000/Voc_1000-1)/log(1-Imp_1000/Isc_1000);
    C_1_1000=(1-Imp_1000/Isc_1000)*exp(-Vmp_1000/(C_2_1000*Voc_1000));
    Voc_m_iterate_1000=C_2_1000*V_oc*log(1+(It_1000/I_sc)/C_1_1000);
end
while V_1000<Voc_1000
    V_1000=V_1000+h;
    c=c+1;
    I_1000=Isc_1000*(1-C_1_1000*(exp(V_1000/(C_2_1000*Voc_1000))-1));
    P_1000=I_1000*V_1000;
    P_1000Plot(c)=P_1000;
```

```
138     I_1000Plot(c)=I_1000;
139     V_1000Plot(c)=V_1000;
140     if I_1000<=0
141         break
142     end
143 end
144 P_tigo_max=max(C_3);
145 P_max_simple=max(P_1000Plot); %[W]
146 [true_simple, column_simple]=ismember(P_max_simple,P_1000Plot,'legacy'
    );
147 V_mpp_simple=V_1000Plot(column_simple); I_mpp_simple=I_1000Plot(
    column_simple);
148 I_mea_C3=4.56; I_mea_C6=1.64; % [A] from Tigo 11.03.20 12:43
149 I_tigo=(I_mea_C3*5+I_mea_C6)/6;
150 V_mea_C3=32; V_mea_C6=36; %[V] from Tigo 11.03.20 12:43
151 % I_mea_C3=7.55; I_mea_C6=1.35; I_mea_C45=7.52; I_mea_C12=7.48;% [A]
    from Tigo 25.05.20 12:01(?)
152 % I_tigo=(I_mea_C3+(I_mea_C12+I_mea_C45)*2+I_mea_C6)/6;
153 % V_mea_C3=29; V_mea_C6=34; %[V] from Tigo 25.05.20 12:01(?)
154 V_mea_C6_string=V_mea_C6*6; V_tigo=V_mea_C3*5+V_mea_C6;
155 %% Plot
156 sz=10; %size of calc MPP
157 figure
158 plot(VPlot,IPlot)
159 hold on
160 plot(V_1000Plot,I_1000Plot)
161 scatter(V_mea_C3,I_mea_C3,'filled')
162 scatter(V_mpp_simple,I_mpp_simple,sz,'k','filled')
163 scatter(V_5,I_5,sz,'k','filled')
164 xlabel('Voltage [V]')
165 ylabel('Current [A]')
166 legend('Single diode model','Simplified Model','IBC poly operational
    point','Location','west')
167 grid;
168 figure
169 plot(VPlot,PPlot)
170 hold on
171 plot(V_1000Plot,P_1000Plot)
```

```
scatter(V_mea_C3,P_tigo_max,'filled')
scatter(V_mpp_simple,P_max_simple,sz,'k','filled')
scatter(V_5,P_max_5,sz,'k','filled')
xlabel('Voltage [V]')
ylabel('Power [W]')
legend('Single diode model','Simplified model','IBC mono operational point','Location','northwest')
grid;
%String from tigo
% figure
% plot(t_halla,C_1)
% hold on
% plot(t_halla,C_2)
% plot(t_halla,C_3)
% plot(t_halla,C_4)
% plot(t_halla,C_5)
% plot(t_halla,C_6)
% legend('C1','C2','C3','C4','C5','C6')
% grid;
figure
plot(VPlot,IPlot)
hold on
scatter(V_mea_C3,I_mea_C3,'filled')
scatter(V_mea_C6,I_mea_C6,'filled')
scatter(V_5,I_5,sz,'k','filled')
%scatter(V_mea_C6_2,I_mea_C6_2,'filled')
xlabel('Voltage [V]')
ylabel('Current [A]')
legend('IV curve','Operating point of unshaded modules','Operating point of shaded module','Calculated MPP','location','southwest')
grid;
figure
plot(VPlot,PPlot)
hold on
scatter(V_mea_C3,P_tigo_max,'filled')
scatter(V_mea_C6,C_6_SI,'filled')
scatter(V_5,P_max_5,sz,'k','filled')
xlabel('Voltage [V]')
```

```
208 ylabel('Power [W]')
209 legend('Power–Voltage curve','Operating point of unshaded modules','
    Operating point of shaded module','Calculated MPP','location','
    northwest')
210 grid;
211 %% From Simulink
212 %V_string=0:6/(1e4):V*6;
213 V_sim_sh=out.Volt.Data; V_string=VPlot*6; %String voltage from
    Simulink and matlab [V]
214 I_sim_sh=out.Current.Data; I_string_shade=(IPlot*5+IPlot*SI_C_6)/6; %
    String current from Simulink and Matlab [A]
215 P_sim_sh=I_sim_sh.*V_sim_sh; P_string_shade=V_string.*I_string_shade;
    P_string_no=V_string.*IPlot;
216 P_sim_sh_max=max(P_sim_sh(81:end)); [true_sim_sh, row_sim_sh]=ismember
    (P_sim_sh_max,P_sim_sh,'row');
217 P_string_shade_max=max(P_string_shade); [true_shade, column_shade]=
    ismember(P_string_shade_max,P_string_shade,'legacy');
218 P_string_no_max=max(P_string_no); [true_no, column_no]=ismember(
    P_string_no_max,P_string_no,'legacy');
219 V_sim_sh_max=V_sim_sh(row_sim_sh); V_string_shade_max=V_string(
    column_shade); V_string_no_max=V_string(column_no);
220 I_sim_sh_max=I_sim_sh(row_sim_sh); I_string_shade_max=I_string_shade(
    column_shade); I_string_no_max=IPlot(column_no);
221 %Plot
222 figure
223 plot(V_sim_sh,I_sim_sh)
224 hold on
225 plot(V_string,I_string_shade)
226 plot(V_string,IPlot)
227 scatter(V_tigo,I_tigo,'c','filled')
228 scatter(V_sim_sh_max,I_sim_sh_max,'k','filled')
229 scatter(V_string_shade_max,I_string_shade_max,'k','filled')
230 scatter(V_string_no_max,I_string_no_max,'k','filled')
231 %scatter(V_mea_C6_string,I_mea_C6,'c','filled')
232 legend('Inverter with string MPPT','Shaded string with P.O.','String w
    .o. shade','Actual operating point','Calculated MPP','location','
    southwest')
233 xlabel('Voltage [V]')
```

```
234 ylabel('Current [A]')
235 ylim([0 I_pv+1])
236 grid;
237 figure
238 plot(V_sim_sh,P_sim_sh)
239 hold on
240 plot(V_string,P_string_shade)
241 plot(V_string,P_string_no)
242 scatter(V_tigo,P_string_C_max,'c','filled')
243 scatter(V_sim_sh_max,P_sim_sh_max,'k','filled')
244 scatter(V_string_shade_max,P_string_shade_max,'k','filled')
245 scatter(V_string_no_max,P_string_no_max,'k','filled')
246 %scatter(V_mea_C6_string,P_C6_string,'r','filled')
247 xlabel('Voltage [V]')
248 ylabel('Power [W]')
249 ylim([0 P_string_no_max+50])
250 legend('Shaded string w.o. P.O.','Shaded string with P.O.','String w.o
       . shade','Actual operating point','Calculated MPP','location','
       northwest')
251 grid;
252 P_lost=P_string_no_max-P_string_shade_max; %Power lost to shade [W]
253 P_pot_lost=P_string_no_max-P_sim_sh_max; %Power potentially lost to
       shade [W]
254 P_rec=P_string_shade_max-P_sim_sh_max; %Power reclaimed [W]
```